DRAL
Daresbury Laboratory
Rutherford Appleton Laboratory

RAL Report
RAL-94-081

NASA-TM-110114

The Location and Characteristics of the Reconnection X-Line Deduced from Low-Altitude Satellite and Radar Observations

M Lockwood C J Davis M F Smith T G Onsager and W F Denig

July 1994

Rutherford Appleton Laboratory Chilton DIDCOT Oxfordshire OX11 0QX

THE LOCATION AND CHARACTERISTICS OF THE RECONNECTION X-LINE DEDUCED FROM LOW-ALTITUDE SATELLITE AND RADAR OBSERVATIONS

M. Lockwood and C.J. Davis
Rutherford Appleton Laboratory, Chilton, Didcot, Oxfordshire, U.K.

M.F. Smith
Laboratory for Extraterrestrial Physics, Goddard SFC, Greenbelt, Maryland, U.S.A.

T.G. Onsager
Institute for the Study of the Earth, Oceans, and Space and Department of Physics, University of New Hampshire, Durham, USA

W.F Denig
Phillips Laboratory, PL/GPSG, Hanscom AFB, Bedford, USA

Abstract.
We present an analysis of a cusp ion step observed between two poleward-moving events of enhanced ionospheric electron temperature. From the computed variation of the reconnection rate and the onset times of the associated ionospheric events, the distance between the satellite and the X-line can be estimated, but with a large uncertainty due to that in the determination of the low-energy cut-off of the ion velocity distribution function, f(E). Nevertheless, analysis of the time series f(t) shows the reconnection site to be on the dayside magnetopause, consistent with the pulsating cusp model, and the best estimate of the X-line location is 13 R_E from the satellite. This is consistent with the field-parallel magnetosheath flow near the X-line which is found to be only 13 $\pm$ 85 km s^{-1}. The ion precipitation is used to reconstruct the field-parallel part of the Cowley-D ion distribution function injected into the open LLBL in the vicinity of the X-line. From this the Alfvén speed, plasma density, magnetic field, parallel ion temperature, and flow velocity of the magnetosheath near the X-line can be derived. In addition, with simultaneous interplanetary or magnetosheath measurements, the magnetic shear across the X-line and the ion transmission factor across the magnetopause rotational discontinuity can also be derived.

1. INTRODUCTION

Cusp ion steps were first predicted by *Smith et al.* [1992] and *Cowley et al.* [1991], based on the pulsating cusp model of the effects of pulsed magnetopause reconnection [*Lockwood and Smith*, 1989; 1990]. Independent of this theoretical work, *Newell and Meng* (1991) published observed examples of such steps. *Lockwood and Smith* [1992] applied their theory to the examples presented by *Newell and Meng* to evaluate the reconnection rate variation. Further examples of these signatures were presented by *Escoubet et al.* [1992] and *Lockwood et al.* [1993a] and were also interpreted in terms of the pulsating cusp model.

As discussed by *Lockwood and Smith* [1994], cusp ion steps can also be produced in steady-state by spatial variations and examples of such have recently been studied by *Onsager et al.* [1994] and *Weiss et al.* [1994]. *Lockwood* [1994b] has discussed how spatial and temporal causes can be distinguished and hence shown that the examples discussed by *Lockwood and Smith* [1989] and *Lockwood et al.* [1993a] were temporal, and not spatial, in origin.

The examples presented by *Lockwood et al.* [1993a] are particularly important as they show the cusp ion steps to lie on the edges of one of a sequence of poleward-moving events, observed simultaneously and in very close conjunction by the EISCAT radars. This is in exact accordance with the pulsating cusp theory. *Lockwood et al.* [1993a] also noted that these combined observations were consistent with the precipitation within each event evolving from cleft to cusp to mantle as the patch of newly open flux produced by the reconnection burst is appended to the tail lobe, as also predicted by the theory [see reviews by *Lockwood*, 1994a; b].

In this paper, we consider in detail the cusp ion step observed by *Lockwood et al.* [1993a] on the equatorward edge of a poleward-moving event, seen simultaneously by the EISCAT radars, and on the cusp/cleft boundary. *Lockwood et al.* used a rough estimate of the magnitude of this step and the repeat period of the events in the EISCAT data to provide an estimate of the location of the reconnection X line. This estimate is refined here and an analysis made of the uncertainties. *Newell and Meng* [1994] have also repeated the calculation of *Lockwood et al.*, but using a different estimate of the size of the step: the analysis presented here is considerably different to both previous studies in both method and results, as will be discussed in the final section. In the section 2 we discuss some important implications of the velocity filter effect for these data, which are described in detail in section 3. In sections 4, 5 and 6 we estimate not only the variation of the reconnection rate and the location of the reconnection X line, but the de-Hoffman Teller velocity in its

vicinity and the distribution function of the ions injected there. This yields estimates of the plasma density, magnetic field and bulk flow, all at the magnetosheath inflow region to the magnetopause X-line.

2. TIME OF FLIGHT EFFECTS

The velocity filter effect

The velocity filter effect of injected cusp ions was first discussed by *Rosenbauer et al.* [1975]; *Shelley et al.* [1976]; *Reiff et al.* [1977] and *Hill and Reiff* [1977]. Ions of different field-aligned velocity, injected simultaneously across the magnetopause onto any one field line have different flight times along that field line. Hence they have different arrival times in the ionosphere and, as the field line is convecting, are spatially dispersed along the locus of the field line. In other words, the trajectories of the ions are only field-aligned if there is no convection and the magnetosphere is stagnant [*Lockwood and Smith*, 1993].

Figure 1 illustrates some important consequences of the velocity-filter effect. Consider a low-altitude satellite, S, which is moving equatorward and convection which is also poleward (but at a speed much greater than the convection speed - see discussion by *Lockwood and Smith* [1994]). The plot shows the variation of the maximum and minimum energies of a detectable flux of magnetosheath-like particles seen by S as a function of observing time, t_s. At any one t_s, the satellite sees ions with a range of energies and hence with a range of field-aligned speeds. At each time, therefore, the satellite observes ions with a range of flight times from the magnetopause and, because the field line (onto which these ions are frozen) is convecting, a range of injection locations [*Lockwood and Smith*, 1993; *Onsager et al.*, 1993]. It is useful to here consider where the spectrum of particles injected onto a field line at any one point P_n on the magnetopause and at a time t_n are detected by the satellite. The higher energy ions of this spectrum at the magnetopause have lower flight times and, because of the poleward convection of that field line, are seen at lower latitudes in the ionosphere (and thus at higher t_s for this example of an equatorward-moving satellite). For scatter-free, adiabatic motion all ions are seen by the satellite with the same energy, E, and (by Loiuville's theorem) phase space density, f, as they had at P_n. The energy and observation time are related by the time-of-flight equation:

$$(t_s - t_n) = d_n(m/2E)^{1/2} \qquad (1)$$

where m is the ion mass and d_n is the distance along the field line from P_n to the satellite. In figure 3, dashed lines (defined by equation 1) join ions sharing the same injection time (and, as the field line is convecting along the magnetopause, they therefore must also share the same injection location). Four such lines are shown, for injection times t_1 to t_4 (marked 1 - 4).

Also shown in this figure are three ionospheric regions of magnetosheath-like particle precipitation, termed "cleft", "cusp" and "mantle". These are defined for each t_s by the density and spectra of the electron and ion precipitation, usually using the classifications devised by *Newell and Meng* [1988] and *Newell et al.* [1991] and employed by *Newell and Meng* [1992]. Notice that any one injection point will usually contribute ions to more than one of these regions and that the ion spectrum seen by the satellite at any one time, t_s, is an ensemble, with different energies coming from different injection locations. In defending their classifications, *Newell and Meng* [1993] state that they do not believe this to be the case, which indicates that their classifications do not make any allowance for the velocity filter effect.

The open magnetosphere cusp model

The above time-of-flight considerations are simply the implications of the velocity filter effect and do not make any assumptions about the mechanism responsible for injecting the magnetosheath plasma across the magnetopause. The evidence that cusp particles enter the magnetosphere along newly-opened field lines, produced by reconnection at the dayside magnetopause, has recently been reviewed by *Lockwood and Smith* [1994] and will not be repeated here. Once a field line is opened, the plasma streams continuously across the rotational discontinuity at the magnetopause. This has been confirmed by applications of the tangential stress-balance test, both on the dayside magnetopause [*Aggson et al.*, 1983; *Paschmann et al.*, 1979; 1986; *Sonnerup*, 1980; 1990] and on the boundary of the near-Earth tail lobe [*Sanchez and Siscoe*, 1990; *Sanchez et al.*, 1990]. Initially, the ions are accelerated on crossing the boundary and flow (along with sufficient electrons to maintain quasi neutrality) towards the Earth, giving the low-altitude (open)cleft, cusp and mantle precipitations. However, after the field line has convected through the magnetic cusp the entering ions are decelerated and flow super-thermally in the anti-sunward direction in the high-altitude mantle. Note, therefore, that although this high-altitude mantle is threaded by the same field lines as the region of low-altitude precipitation also termed mantle, the latter precipitation does not arise from the former population: by the time that the few Earthward-directed ions in the high-altitude mantle reach the ionosphere, the field line has convected into the polar cap and ions from the high altitude mantle form a low-density, low-energy (in the Earth's frame of reference) precipitation in the ionospheric polar cap.

The evolution of a newly-opened field line and the corresponding examples of the injected ion distribution are illustrated schematically in figures 2 and 3, respectively. In figure 2, the satellite S is shown in the northern hemisphere topside ionosphere, making observations on a newly-opened field line which is in the position labelled 4. The diagram shows

three earlier positions of that newly-opened field line as it evolves from the X-line towards the tail lobe: position 1 is shortly after the field line was reconnected at the X-line, X; in position 2 it threads the magnetopause at higher latitudes on the dayside; and in position 3 the field line is approaching the magnetic cusp. Ions injected with the field line in these four positions are dispersed along the corresponding dashed lines marked 1-4 in figure 1. In figure 2, we have deliberately placed X away from the magnetic equator to stress that the field-aligned distance between X and S, d, is variable. We would expect d to vary with the Earth's dipole tilt (i.e with season and time of day) as well as with the IMF orientation and the solar wind dynamic pressure.

At all the four field-line locations (and all those between them) magnetosheath plasma streams continuously across the field line rotational discontinuity (RD) at the magnetopause. The theory of *Cowley* [1982] predicts that the injected ions form an open low-latitude boundary layer (LLBL) and that they will show a characteristic D-shaped ion velocity distribution. These predictions have recently been borne out in considerable qualitative and quantitative detail by *Smith and Rodgers* [1991], *Gosling et al.* [1990b; c], *Fuselier et al.* [1991] and *Lockwood et al.* [1994]. *Gosling et al.* [1990b; c] found the characteristic D-shaped distributions, the field-parallel part of which has been reconstructed from cusp/cleft ion precipitation by *Lockwood et al.* [1994]. *Smith and Rodgers* [1991] showed that the low-velocity cut-off of the D was close to the de-Hoffman Teller velocity, as determined from the stress-balance test and *Fuselier et al.* [1992] showed that all distributions, on both sides of the boundary, were also as predicted by *Cowley*. Figure 3 shows the truncated, drifting maxwellian shapes of the field-parallel part of distribution functions, f(v), injected across the boundary when a field line is in the 4 positions shown in figure 2. Near the X-line (position 1) the cut-off velocity of the injected population is V_{FX}, the local de-Hoffman Teller velocity, and the bulk drift is V_{pl}. The other 3 locations are further removed from the X-line the magnetosheath temperature and density are both progressively reduced in this figure. *Lockwood and Smith* [1994] have shown that both the minimum and peak velocity of the injected distribution increases as the field line accelerates away from the X-line, and this is reflected in figure 3 for the distribution injected when the field line is position 2. However, as the field line approaches the magnetic cusp, the RD straightens and *Lockwood and Smith* predict that both the lower cut-off and peak velocity will decrease again. The position 3 in figures 1-3 is a special one, in that it is where the minimum velocity of the injected distribution returns to its value at the X-line, V_{FX}. By the time the field line has evolved to position 4, the RD has become an obtuse rather than an acute angle and the ion acceleration on crossing the magnetopause has turned to a weak deceleration.

Each and every newly-opened field line undergoes the evolution shown

in figure 2, and hence each has the sequence of distributions shown in figure 3 injected onto it. We are only concerned with the field-parallel part of the injected distribution, all other pitch angles being mirrored in the converging magnetic field lines before reaching S. If the reconnection rate is steady, as S flies equatorward it would sample field lines which were reconnected increasingly later (i.e. the elapsed time since reconnection continuously decreases). In figure 1, the line marked 1 is where magnetosheath ions are last seen at each energy by the equatorward-moving satellite. Hence for every observation time t_s, the time t_1 is when ions are first injected across the magnetopause onto that field line (i.e. they are opened at time t_1 and the point P_1 is the reconnection site). Prior to it being opened at t_1, no ions were injected and hence t_1 is a minimum of t_n, which by equation (1) yields a minimum of the ion energy, E, which we call the "lower cut-off" energy, E_{ic}.

The theory of *Cowley* [1982] shows that near the X-line, the minimum injected ion speed is almost the local de-Hoffman Teller velocity, V_{FX}. This means that the field-parallel ion spectrum injected near the X-line has a minimum energy very close to $(mV_{FX}^2/2)$. This was confirmed by *Smith and Rodgers* [1992] using the stress-balance test. Those ions are dispersed along the line marked 1 in figure 1, given by equation (1) for d_n equal to the distance between the satellite and the X-line, d_1, which we henceforth will abbreviate to d. However, because there is a minimum energy injected at the X-line, particles are only seen along the line 1 down to the point A, at an energy of $(mV_{FX}^2/2)$, and no particles are seen from the X-line (by the equatorward-moving S) before t_A, the value of t_s the point A.

The line marked 2 joins the spectra of ions injected onto each newly-opened field line at an elapsed since it was reconnected of $(t_2 - t_1)$. This injection will take place at a point P_2, at a higher magnetic latitude because the field line evolves poleward at the de-Hoffman Teller frame speed, V_F (which is typically 100-300 km s^{-1}, corresponding to a field-perpendicular convection velocity of typically 10-30 km s^{-1}). The model of *Lockwood and Smith* [1994] shows that as the field line accelerates away from the reconnection site (V_F rises) the minimum injected energy (equal to $mV_F^2\cos^2\theta_{sp}/2$) rises. The model also shows that the minimum injected energy does not fall below $(mV_{FX}^2/2)$ until the field line is close to the magnetic cusp when the angle that the magnetospheric file makes with the magnetopause, θ_{sp}, becomes larger as the newly-opened field line straightens. Figure 1 is drawn such that this happens at the point P_3, which is a field-aligned distance d_3 from the satellite, and the spectrum injected here is spread along the line 3. Hence in the ionosphere ions from P_3 are seen down to the point B along the dashed line marked 3.

At elapsed times since reconnection greater than $(t_3 - t_1)$, the minimum injected energy falls below $(mV_{FX}^2/2)$ and lower energy ions are seen in the ionosphere. The line marked 4 joins the spectrum of ions injected

from a point P_4, yet further along the locus of the newly-opened field lines over the magnetopause as they evolve from the X-line into the tail lobe.

Figure 3 also illustrates some important points about the spectrum of particles observed at any one observation time, t_s. The solid circles mark the parts of the distributions 1 and 2 which arrive simultaneously at S, at a t_s which is comparatively late in the pass (when S is in the region classed as cleft in figure 1). The dashed line joining them is the rest of the spectrum observed at that time. The largest f observed is from the X-line, and is at a velocity immediately above the time-of-flight cut-off. The squares are the parts of distributions seen at an earlier t_s, (when S is in the cusp region in figure 1) and the dotted line shows the full distribution observed at that time. Note at this earlier t_s, the field line is observed at much larger time since reconnection and the time-of-flight cut-off velocity is much lower. Unlike for the dashed line, in this second case the largest f is not at a velocity just above the cut-off and comes from the mid-latitude magnetopause rather than the X-line. Comparison of these two spectra shows that the peak f observed at any one t_s does not bear a fixed relationship with the cut-off and hence cannot be used to define the cut-off. The only exception to this is nearer the open-closed boundary where the peak f and the cut-off are both at greater velocities and almost at the same velocity (as in the dashed line in figure 3).

Implications for the DMSP-F10 pass on 28 March 1992

There are a number of important points to be derived from figure 1 which are relevant to the analysis of the DMSP-F10 pass presented in the next section. It is important to note that this pass is equatorward, as in the schematic in figure 1. (Note that for poleward passes, the t_s axis is reversed).

Firstly, there will be a low-energy cut-off, E_{ic}, for ions. For $E_{ic} > (mV_{FX}^2/2)$, all ions at this cut-off originated from the X-line (a distance d from the satellite). Lower cut-off ions of energy $E_{ic} < (mV_{FX}^2/2)$ come from the points near the magnetic cusp (and a field-aligned distance of roughly $d_3 \approx d_c$ from the satellite) [*Lockwood and Davis*, 1994]. Between the points A and B there is an interesting feature, which reflects the increase in the minimum injected energy (as the field line accelerates away from the X line) and its subsequent decay (as the rotational discontinuity at the magnetopause straightens out), as recently predicted by *Lockwood and Smith* [1994]. This effect is countered somewhat by the fact that the distance from the satellite to the injection point falls with time (from d to d_3) as the field line evolves away from the X-line. In this paper we present observation in which we identify the point A, giving the de-Hoffman Teller velocity at the X-line V_{FX}, using the procedure adopted by *Lockwood et al.* [1994].. To do this we note that the

equatorward-moving satellite would, at an energy just greater than $(mV_{FX}^2/2)$, cut the E_{ic} contour three times, whereas for $E_c >> (mV_{FX}^2/2)$ or $E_d < (mV_{FX}^2/2)$ it would cut it just once. At the energies close to, but greater than, $(mV_{FX}^2/2)$ the equatorward-moving satellite would observe a decay in the flux of magnetosheath-like ions at observation times t_s soon after the time t_B, followed by a rise just before t_A and a final fall just after t_A. At energies below $(mV_{FX}^2/2)$ (like E_d in figure 1), the satellite would see a single fall in ion flux at a time t_d before t_B, whereas at energies well above $(mV_{FX}^2/2)$ (like E_c in figure 1) it would see a decay at $t_c > t_A$.

We note in passing that features like that between t_A and t_B in figure 1 appear to be quite common in cusp passes and hence the techniques employed later in this paper could be used to analyse the magnetosheath conditions at the reconnection site for a considerable number of passes [see also *Lockwood et al.*, 1994]. The difficulty in detecting the predicted feature is that ions of higher energy may be scattered to lower energies near the satellite, making the minimum between t_B and t_A difficult to detect. Because of these scattered ions at low energies, the predicted feature should be much easier to detect if V_{FX} is large.

The second important point to remember concerns the spectrum of particles observed at any one observation time t_s. The velocity filter effect means that this is an ensemble of particles, with the more energetic ions coming from injection points further removed from the reconnection site, compared with the lower energy ions seen at the same time. As demonstrated by figure 3, taking measurements at a constant energy within the magnetosphere means that the changing ion acceleration causes one to effectively sample a different part of the f(v) in the magnetosheath. This spatial factor, along with the temperature and density variations in the sheath, are included in figure 3. The important conclusion is that the energy of the peak of a the spectrum (here called E_p) bears no fixed relationship with the low-velocity cut-off (and hence E_{ic}): although the two are close at high energies, E_{ic} will fall well below the E_p at lower energies, as in the two examples in figure 3.

3. COMBINED SATELLITE AND GROUND-BASED OBSERVATIONS ON 28 MARCH 1992

On 28 March 1992, the DMSP-F10 satellite intersected the cusp region when in very close conjunction with the EISCAT radars, operating in the SP-UK-CONV mode. *Lockwood et al.*, [1993a] have described this conjunction and the reader is referred to their paper for fuller details. The EISCAT UHF radar is pointed along the magnetic meridian and the DMSP-F10 satellite crossed it moving equatorwards and to the west. At the poleward edge of the cusp, the DMSP-F10 satellite was at an MLT just ΔMLT = +9 min greater than that of the EISCAT UHF radar range gate at the same invariant latitude. The corresponding value at the

equatorward edge of the cusp was ΔMLT = -6 min and at the equatorward edge of the cleft (open LLBL) ΔMLT was - 9 min. Hence this conjunction is very close indeed.

Both the EISCAT UHF and VHF radars on this day saw a sequence of poleward-moving electron temperature enhancements. A continuous sequence of eleven such events were seen in a 90 min period. This yields a mean repeat period of nearly 8 min., which is interestingly close to the mean period of other transient events in the cusp and at the dayside magnetopause, namely poleward-moving auroral forms [*Fasel*, 1994] and FTE signatures [*Rijnbeek et al.*, 1984; *Lockwood and Wild*, 1993], respectively. These electron density enhancements were not accompanied by any depletions in the plasma density and hence revealed an additional heat source for the ionosphere. Between the boundaries of the cusp region, defined from the DMSP-F10 data using the criteria used by *Newell et al.* [1991], EISCAT observed a region of high electron temperature, consistent with previous observations of elevated electron temperatures in the cusp region [*Titheridge*, 1976; *Brace et al.*, 1982; *Curtis et al.*, 1982; *Wickwar et al.*, 1974; *Wickwar and Kofman*, 1984; *Waterman et al.*, 1994]. However, being from ground-based remote sensing observations of much higher time resolution (10-seconds with no antenna scanning), the observations presented by *Lockwood et al.* [1993a] were the first to show that the electron temperature enhancement was not steady, but was just one of the continuous series of poleward-moving events.

Figure 4 shows the three events observed by the EISCAT UHF radar around the time of the satellite pass. The arrows point to the locations where DMSP-F10 observed cusp ion steps bounding the region defined as cusp. This figure shows the electron temperature in grey scale, as a function of invariant latitude and UT. The vectors show the plasma flow derived by combining the line-of-sight velocities from the UHF and VHF radars. For the SP-UK-CONV experiment, the UHF radar points along the magnetic meridian and hence, to within a small uncertainty due to field-aligned flow, measures the northward convection component directly. The east-west component is less certain because it is derived by comparing the line-of-sight velocities from the two radars and assuming that the flow is constant along L-shells over the spatial separation of the two beams: however, this component is not employed in the present paper. The northward component of the flow, V_N was roughly 500 m s^{-1} at all times and locations observed. There are a weak enhancements (of about 100 ms^{-1}) at all latitudes at the onset of each T_e event and a weak enhancement (also of about 100 ms^{-1}) which propagates poleward with each event around its equatorward edge.

The electron temperature event seen by EISCAT which was co-incident in time and space with the cusp precipitation (as seen by DMSP-F10) had an onset at around 10:10 UT. Poleward of this was another event, in what

the satellite defined to be the mantle region. The (open)cleft precipitation region observed by the satellite evolved into a third event which was first observed just before 10:14UT. *Lockwood et al.* [1993a] point out that the EISCAT data reveal the cleft, cusp and mantle regions defined by the satellite to be the same type of poleward-moving event, simply seen at different phases of their evolution. *Lockwood and Smith* [1993] note that this is also consistent with the velocity filter effect discussed in section (2).

Figure 3 of *Lockwood et al.* [1993a] provides an overview of the electron and ion data from the DMSP-F10 satellite during this pass. The ion data have 1-second integration times for each energy channel. The instrument has two channels near 955 eV (with different geometric factors) which are averaged together here. The calculations of distribution function $f(E,t_s)$ and differential energy flux $J_E(E,t_s)$ from the instrument count rates assumes that there is an isotropic downward flux of protons. From 10:10:58 until 10:11:15 the satellite is in the region which would be classified as cusp. As the satellite moves equatorward from this point, the energies of peak J_E and f increase until 10:11:22, when the values of J_E and f fall to the background fluctuation level and there is no evidence of any magnetosheath-like ion precipitation. Between 10:11:15 and 10:11:22 there are clear indications of a low-energy cut off, E_{ic}, of the spectrum, but this does not rise in a uniform manner. The nature of this rise is one of the main considerations of this paper.

The question then arises as how to best determine the value of E_{ic} at each observation time t_s. The problem is that scattering may smear this time-of-flight cut-off and make it difficult to define. In addition, aliasing will smear this cut-off if there are significantly changes in the spectrum within the 1-second integration time of the instrument. In their paper, which employed $E_{ic}(t_s)$ to compute the variation of the magnetopause reconnection rate, *Lockwood and Smith* [1992] used the energy where the differential energy flux fell to a tenth of its peak value, an approach which has also been adopted by *Newell and Meng* [1994]. *Lockwood and Smith* did note that this definition was somewhat arbitrary, but found that other definitions did not alter their main result, namely that nearly all the reconnection came in three short pulses for the pass that they studied. However, in the present paper we wish to make further deductions from $E_{ic}(t_s)$ and the effect of employing any arbitrary definitions has to be studied in detail. We wish to make two points about the definition employed by both *Lockwood and Smith* and *Newell and Meng*. Firstly, E_{ic} will be employed with time-of-flight considerations and hence it is important to use the velocity space density (distribution function), $f(E,t_s)$, to define E_{ic} and not the differential energy flux, $J_E(E,t_s)$. The latter is proportional to (fE^2) and hence accentuates features at high energies and suppresses those at lower energies. Secondly, it is not correct to fit the spectrum at any one t_s to define E_{ic}. This is because, as discussed in section 2, the velocity filter effect results in the spectrum at any one t_s

being made up of ions from a variety of points on the magnetopause and hence is distorted by spatial variations in the magnetosheath ion temperature and density along the magnetopause and by the variation of the ion acceleration factor on crossing the magnetopause as the field lines accelerate and straighten. As a result, and as demonstrated by figure 3, the peak f (or J_E) has no bearing on the value of E_{ic} and definitions of the type used by *Lockwood and Smith* and *Newell and Meng* should not be used. Instead, we here not only inspect plots of f(E) for every observation time t_s, but also plots of $f(t_s)$ for every energy channel of the instrument (i.e. at constant E).

As there is, at this stage, no obvious way to estimate the low-energy cut-off, E_{ic}, we here adopt a number of different definitions, shown in figure 5. In the remainder of this section and in later sections we discuss these estimates of E_{ic} and which is the most reliable.

The three panels of figure 6 give f(E) on logarithmic scales for four times, one second apart, in each panel. The last spectrum in each panel (solid line) is repeated as a dotted line in the subsequent panel to allow comparison. For each panel the one-count level is plotted as a solid line, with a step near 0.1keV due to the discontinuous change in the instrument geometric factor. The low energy cut-off E_{ic} is clearest at the equatorward edge of the cusp and hence is easiest to follow its variation by considering the last spectrum shown (for 10:11:23) first. At this time, f(E) shows a clear peak at 2.98 keV but drops to the one-count level in the energy bin below this peak. Hence between these two bins there is a sharp fall in f(E) with decreasing E, in other words the low-energy cut-off E_{ic} lies between the two. We here use the nomenclature that E_1 is the centre of the energy bin in which f(E) falls to or below the one-count level and that E_p is the centre of the energy bin detecting peak f. The best estimate of E_{ic} from the f(E) spectra we term $[E_{ic}]_E$ and is $(E_1 + E_p)/2 \pm (E_1 - E_2)/2$. For all distribution functions in figure 6c, E_1 and E_p are just one energy bin apart and rise with t_s. This rise is also seen in figure 6b, but is much more rapid, with E_1 rising with t_s from 96 eV at 10:11:17 to 1.38 keV at 10:11:20 while in the same period E_p rises from 950 eV to 2.03 eV. Because of this rapid change, the form of the distribution function at 10:11:19 is distorted by the effect of aliasing as E_{ic} rises rapidly. In other words, at the end of this 1-second integration period, the detector is no longer seeing lower energy ions which were present at its start.

Because of the non-subjective definitions of E_1 and E_p, they could be computed by an automated algorithm. Only one subjective decision was required because at 10:11:18 f(E) never falls to the one-count level. However, this is due to one or two background counts at the lowest energies which may well have resulted from scattering. Similar low-level counts were seen below the defined E_1 in the subsequent two spectra. At 10:11:18, a clear decay to this background level can be defined and from

this E_l was taken to be 140 eV.

Figure 6a shows that the spectrum changes relatively slowly poleward of the rapid rise shown in figure 6b.

Figure 5 shows E_l (dashed line), E_p (dot-dash line) and $[E_{ic}]_E$ (solid line) as a function of observation time, t_s, which is here defined to be zero at 10:08:00. All three reveal the cusp ion step around t_s = 199s, as identified from the spectrogram by *Lockwood et al.* [1993a]. At the higher energies (after 10:11:20) there is little doubt about the validity of this estimate for E_{ic} because E_p and E_l are just one energy bin apart, as in the dashed line in figure 3. However, before this time there is a much larger uncertainty because E_p and E_l are several energy bins apart (as in the dotted line in figure 3). In this paper, we obtain further information about E_{ic} by studying the variation of f with observation time, t_s, for each energy bin. The results are shown in figure 7.

As in figure 6, the solid trace in one part of figure 7 also appears as a dotted trace in the next to allow comparisons. Note that figure 7a is for an interval 6s earlier than for parts b, c, and d. Without scattering or aliasing, the value of $f(t_s)$ for each energy channel would vary as the satellite traversed the mantle/cusp/cleft region but would encounter a sudden drop to the one count level (when E_{ic} rose above the energy of the channel) as the satellite emerged on the equatorward side of the cusp/cleft region. Figure 7 shows that this decay is usually clear but not sudden: as a result, the time that E_{ic} equals the energy of that channel can be determined, but with some uncertainty. The decay occurs later at higher energies, as expected. However, figures 7b and 7c show that the decay is almost simultaneous at all energy channels between 300 eV and 1.38 keV. This is because of the cusp ion step shown in figure 5. In these cases, the decay to the background fluctuation level of f equatorward of the cusp occurs in just one or two integration period and the uncertainty in the t_s when $E = E_{ic}$ is therefore only $\pm$ 0.5 s or $\pm$ 1.0 s, respectively. The horizontal bars in figure 5 show the times of this decay at each energy level, as scaled from figure 7, and the open circles represent the times at the centre of each decay.

It is useful to compare these times (when E_{ic} crosses the energy E of each instrument channel) with the plotted variations of E_p, E_l and $[E_{ic}]_E$. It is clear that E_l agrees quite well if E_{ic} is taken to be at the end of the decay in $f(t_s)$, whereas E_p agrees well if E_{ic} is taken to be at the start of each decay, confirming that these two are extreme limits for E_{ic}. In the next section, we show that the conclusions of *Lockwood et al.* [1993a] and *Newell and Meng* [1994] are critically dependent on how E_{ic} is defined. To emphasise this, in figure 5 we give two estimates of $E_{ic}(t_s)$, both midway between the two extremes of E_l and E_p. The solid line is $[E_{ic}]_E$, as defined above, whereas the dashed line is a second estimate defined from the $f(t_s)$ plots, which we term $[E_{ic}]_T$. These are the 1-second

values which give a variation which is a best fit to the open circles. In section 4 we will employ both estimates to illustrate the sensitivity of any deductions to the choice of how E_{ic} is estimated.

4. THE VARIATION OF THE RECONNECTION RATE

The equations derived by *Lockwood and Smith* [1992] can be applied to the variations of the various estimates of the low-energy cut-off, E_{ic}, discussed in the previous section. Specifically, the reconnection rate at the magnetopause X-line is given by:

$$\varepsilon_y(t_l) = (B_i\ V_s \cos\alpha)\ (dy/dy')\ \{1 + (d/2)\ (m/2)^{1/2}\ E_{ic}^{-3/2}\ dE_{ic}/dt_s\}^{-1} \quad (2)$$

where B_i is the ionospheric magnetic field; V_s is the satellite velocity in the Earth's frame (which is positive away from merging gap and at an angle α with respect to it); (dy/dy') is the one-dimensional magnetic field mapping factor (dy is an element of length along the magnetopause X line and dy' is the corresponding length along the ionospheric merging gap) and d, m and E_{ic} are as defined above. The reconnection rate calculated by (2) is for a time t_l given by equation (1) for $d_n = d$ and hence $E = E_{ic}$.

The value of ε_y derived depends sensitively on the temporal gradient of E_{ic} and its uncertainty is set by the energy resolution of the instrument. As pointed out by *Lockwood and Smith* [1992], the measurement errors are very large when the reconnection rate is large. To understand this note that when ε_y is large, dE_{ic}/dt_s is small and can be even negative. A small error in the experimental determination in this gradient can then cause the estimated ε_y to be infinite or even negative. However if ε_y is small, dE_{ic}/dt_s is large and errors in its experimental estimation have little effect on the estimated ε_y. As a result, the method does not give reliable absolute estimates of the magnitude of the reconnection rate pulses, at least with ion data of the energy resolution presented here. However, it does show the waveform of the ε_y variation and clearly differentiates between periods of very high and very low reconnection rate. Another feature to note about equation (2) is that the value of ε_y does not only depend on dE_{ic}/dt_s, but this term is multiplied by a factor $E_{ic}^{-3/2}$. Hence periods of low ε_y give steep gradients in the cut-off energy E_{ic} when it is large, but much less obvious gradients when E_{ic} is low. Hence, although visual inspection of cusp ion steps in any series of estimates of E_{ic} (as used by *Lockwood et al.* [1993a] and *Newell and Meng* [1994]) will reveal periods of low reconnection rate, the full duration of those low-rate periods is not determined unless equations (1) and (2) is used to compute $\varepsilon_y(t_l)$.

Figure 8 shows the variation of reconnection rate with time, deduced using the two estimates $[E_{ic}]_E$ (solid line) and $[E_{ic}]_T$ (dashed line), as described in the previous section and shown in figure 5. Both plots assume a field-aligned distance d from the satellite to the X-line of 16 R_E. The analysis is not extended back to periods before 10:11:14 because, as discussed in the next section, we infer this to be the time that E_{ic} decays to the point A. However, this is sufficient to show the end of the reconnection pulse which gave rise to the cusp precipitation and the pulse which gave the cleft precipitation. Figure 8 demonstrates how a small change in the estimate of E_{ic} makes a large difference to the estimated timing of the first pulse. This is because even very small changes in the energy of low-energy ions produces large changes in their flight time and hence in t_l. At higher energies, the flight time is not so sensitive and the timing of the second pulse is much more precisely defined.

Lockwood and Smith [1992] point out that the other factor which strongly influences the timing of the pulses is the assumed value for the distance d. This is illustrated here by figure 9, which uses the estimates of $[E_{ic}]_E$ with values for d of 8 and 22 R_E. The timing of both reconnection pulses is altered, but that of the first pulse is particularly influenced, for the same reasons as described above.

5. THE DISTANCE TO THE RECONNECTION X-LINE

As pointed out by *Lockwood et al.* [1993a], The variations of ε_y can be compared with the EISCAT observations of the poleward moving events to estimate the distance d from the X-line to the satellite.

The period of low reconnection found in figures 8 and 9 arises from the steep rise in the estimates of E_{ic} (between t_s of 198 s. and 200 s. in figure 5) and from the period of more gradual rise before it (between 195 s. and 198 s.). The latter period only gives low ε_y because E_{ic} is low, which is relevant because of the $E_{ic}^{-3/2}$ factor in equation (2). This period (195-200s after 10:08:00) is exactly when the satellite is between the second poleward-moving event seen by EISCAT in figure 4 and the region which later evolves into the third event. Hence we can unambiguously associate the two pulses in the reconnection rate with the second and third events in figure 4. This constrains the value of d, as not only the interval between the two points must be matched, but each reconnection pulse must be a certain time ahead of the appearance of the corresponding EISCAT event. This delay will in part be due to the flight time of the ions, but will also reflect the rise time for the heating of the ionospheric electron gas. There is no reason to expect this delay to be different for the two events. This concept of the delay between the reconnection rate pulse and the appearance of the resulting event in the EISCAT data is the best way to estimate d.

Figure 10 plots this delay as a function of the assumed distance d, and using four estimates of E_{ic}: E_1 (dotted lines); E_p (dot-dash lines); $[E_{ic}]_T$ (dashed lines) and $[E_{ic}]_E$ (solid lines). In each case two lines are shown, the steeper one of each pair being for the first reconnection pulse (the timing of which is a more sensitive function of d, as shown by figure 9) and the other being for the second pulse. Assuming that this delay is the same for the two events, where a pair of lines cross gives the value of the delay. More importantly, it also gives the distance d if we assume that the two pulses are reconnected at the same site. The delays required between the reconnection pulse and the appearance of the event varies from 3.5 min for E_1 to almost 8 min. for E_p. The values of around 5 min. for the other two estimates are highly plausible.

The use of the one-count level, E_1, yields a d of about 6 R_E, which would only be on the magnetopause (at the local cusp) for a highly compressed dayside magnetosphere. The d obtained by using the peak of the distribution function, E_p is about 32 R_E which places the reconnection site somewhere close to the magnetic cusp in the opposite hemisphere for a weakly compressed magnetosphere. As these two should be regarded as extreme limits of the range of E_{ic}, we can conclude that the data are consistent with a reconnection site which was somewhere on the dayside magnetopause.

The estimates $[E_{ic}]_E$ and $[E_{ic}]_T$ yield d of 22 R_E and 13 R_E. The fact that scattering increases counts at energies below E_{ic} means that the energy at the one-count level, E_1, is a poor estimate of E_{ic} and hence the d of 6 R_E can be disregarded. However, comparison of figures 3 and 5 provides an indication why $[E_{ic}]_T$ is more reliable than $[E_{ic}]_E$. Figure 3 demonstrates how E_p and E_{ic} should be similar at high values (as in the dashed, cleft-like spectrum), but how E_p will be considerable greater than E_{ic} when E_{ic} has fallen to low values (as in the dotted cusp-like spectrum). Figure 5 demonstrates that $(E_p - [E_{ic}]_E)$ remains almost constant, which is therefore inconsistent with figure 3, whereas $(E_p - [E_{ic}]_T)$ increases with decreasing E_p, as required by figure 3. In addition, in the next section, we show that only $[E_{ic}]_T$ makes the $f(t_s)$ variations shown in figure 7 consistent with the predictions in figure 1. As a result, we conclude that the best estimate for d is $13R_E$.

6. THE COWLEY-D DISTRIBUTION FUNCTION AT THE RECONNECTION SITE

Of the Cowley-D ion velocity distribution function of magnetosheath ions injected very close to the reconnection site, only the field-parallel (low pitch angle) part will precipitate to the ionosphere. As explained in section (2), they will form the low-energy ion cut-off, $E_{ic}(t_s)$, in the ion spectrogram detected by a low-altitude satellite, for all locations equatorward of A in figure 1. For adiabatic scatter-free motion, both

the energy, E_{ic}, and, by Loiuville's theorem, $f(E_{ic})$ will be conserved on travelling from the X-line to the satellite. Hence, by taking the values of $f(E_{ic})$ at various observation times, t_s, we can re-construct the field-parallel part of the Cowley-D distribution injected near the X-line. This is similar to the procedure adopted by *Hill and Reiff* [1977], but significantly different because they applied it to the peaks of the spectrum seen at each t_s, whereas we require the lower cut-off, which as shown by figure 3, are only the same thing at high energies and can be considerably different at lower energies. This procedure has also been employed recently by *Lockwood et al.* [1994] to analyse the seemingly steady-state pass modelled by *Onsager et al.* [1993]. The values of $f(E_{ic})$ are well defined by figure 7, by taking the value of $f(t_s)$ for each energy channel, immediately before the onset of the decay in f as the satellite travelled through the equatorward boundary of the magnetosheath-like precipitation. Inspection of figure 7 shows that $f(t_s)$ for most E is usually quite steady prior to the decay, hence this is a good estimate of $f(E_{ic})$. The results are shown by the open circles in figure 11. Later in the crossing, when E_l and E_p are just one channel apart (see figure 3), $f(E_p)$ values derived from figure 6 are also good estimates of $f(E_{ic})$ and these are also shown in figure 11, as crosses. Figure 11 reveals that this procedure produces a consistent distribution function, which is very close in form to a drifting Maxwellian. The data point which is furthest from this form is that at the peak, and is taken near the steepest gradient of the step in the E_{ic} estimates (figure 5) where both E_{ic} and $f(E_{ic})$ change rapidly. This data point is therefore likely to have been influenced by aliasing. Note, however, that when least-squares fitting this re-constructed spectrum, all points were given equal weight.

The dot-dash line in figure 11 is the best-fit Maxwellian distribution to these points. This distribution has a field-aligned bulk flow speed of, V_p, of 385 km s^{-1}, a field-parallel ion temperature of $T = 3.1 \times 10^6$ K and a density of $N = 1.3A \times 10^7$ m^{-3}, where A is the ion anisotropy [see *Hill and Reiff*, 1977]. The least-squares fitting gives an uncertainty in V_p of $\pm$ 30 km s^{-1}.

In figure 11, the dot-dash line has been truncated at the energy of 300 eV, corresponding to a velocity of 199 km s^{-1} for protons. In the theory of *Cowley* [1982] this velocity is equal to $(V_{FX}\cos\theta_{sp})$ where V_{FX} is the de-Hoffman-Teller velocity close to the X-line (i.e. the speed of flow in the X-line outflow region) and θ_{sp} is the angle that the newly-opened field lines make with the magnetopause on the magnetospheric side of the rotational discontinuity. This estimate for $(V_{FX}\cos\theta_{sp})$ comes from an analysis of figure 7, as presented for another pass by *Lockwood et al.* [1994].

To understand this estimate of the minimum injected velocity at the X-line, we refer back to section (2) and the predictions for the behaviour

of $f(t_s)$ for energies close to, but greater than the energy of the point A in figure 1. For E of 206eV, 300eV and 440eV, figure 7b shows a fall and then a rise in f at times t_s between 191s to 195s, just before the main decay at t_s between 198s and 200s. This minimum is predicted in figure 1 between t_A and t_B for energy channels close to $(mV_{FX}^2/2)$. The fall is not to values as low as observed after the main decay. We explain this as being due to the fact that at these earlier times there is considerably more flux of ions at greater E and hence more ions will be scattered to be detected by these lower E channels. As predicted, this feature is not seen at E of 650eV or above, where there is simply a decay in f after the inferred time t_A. Similarly, below these energies the decay in f occurs before t_B. For example at 140 eV, there are low values of f at t_s of 192-195s (similar to those seen at this time at 206 eV and 300 eV and which we therefore attribute to scattering), and these decay gradually between 196 and 200 s, with the decay of f at higher energies, rather than with the rise in E_{ic} estimates (as expected if these are scattered ions). However, figure 7a shows that f for E=140 eV also falls from values as large as $10^{9.5}$ $m^{-6}s^3$ between 184 and 187s, i.e. prior to the inferred time $t_s = t_B$. Hence this behaviour is exactly as predicted in section 2 for such an equatorward-moving pass, with the added complication that some scattered particles are detected between t_A and t_B.

From the above, we see that the energy of point A is clearly below 300 eV, and above 140 eV. The variation of $f(t_s)$ at 206 eV implies that it is close to but just above the energy of the point A. We here take 206 eV to be the best estimate of this energy, but allow an uncertainty range of 140-300 Ev. For protons, this yields a value of $(V_{FX}\cos\theta_{sp})$ of 199 km s^{-1} ± 40 km s^{-1}. The best-fit distribution in figure 11 employs the corresponding minimum injected energy of 206eV. This value is also our best estimate of E_{ic} for $t_s = t_A = 195$s. This is significantly less than $[E_{ic}]_E$ at this t_s but very close to the value of $[E_{ic}]_T$. Hence this further strongly supports the estimate of d = 13 R_E derived using $[E_{ic}]_T$. Indeed we can say that, in order to explain the observed variations of $f(t_s)$ at fixed energies, the X-line must be placed a distance d= 13R_E from the satellite.

The estimates of the field-parallel velocities at the peak f and cut-off of the Cowley-D distribution injected at the X-line contain a very important implication. To give field parallel flow into the magnetopause RD at the Alfvén speed, V_A, as required for a time-stationary, one-dimensional ideal-MHD rotational discontinuity used to predict the Cowley-D distributions [*Cowley*, 1982], we require:

$$V_F - V_{sh} = V_A \cos\theta_{sh}, \qquad (3)$$

where V_{sh} is the field-aligned magnetosheath flow velocity along the magnetopause and θ_{sh} is the angle that the magnetosheath field makes

with the magnetopause [*Cowley and Owen*, 1985]. This gives a peak f of the Cowley-D distribution at a speed V_p [*Cowley*, 1982], where:

$$V_p = V_F \cos\theta_{sp} + V_A \qquad (4)$$

From (3) and (4) we get:

$$V_{sh} = V_F + (V_F \cos\theta_{sp} - V_p)\cos\theta_{sh} \qquad (5)$$

The boundary-normal field at the RD, B_n, is small and to a good approximation $\cos\theta_{sp} = \cos\theta_{sh} = 1$. For example, a (very large) boundary-normal field of $B_n = 10$nT, along with magnetosheath and magnetosphere fields of 50 nT gives $\theta_{sp} = \theta_{sh} = \sin^{-1}(0.2) = 11.5°$ and hence $\cos\theta_{sp} = \cos\theta_{sh} = 0.98$. In this case, to a very good approximation we can write

$$V_{sh} = 2V_F - V_p \qquad (6)$$

Above we derived a value for V_p of 385 ± 30 km s^{-1} and for V_F of 199 ± 40 km s^{-1} for the Cowley-D distribution injected in the vicinity of the X-line. From equation (6), this gives us an estimate of the field-parallel sheath flow velocity at the X line of $V_{shX} = 13 \pm 85$ km s^{-1}. This is a highly significant result, as it places the X-line either very close to the subsolar point, where the flow goes to zero, and/or aligns it with the magnetosheath flow streamline which is normal to the magnetosheath field.

It is valuable to compute some other variables at the X-line, in order to check that the above values are sensible. *Cowley* [1982] assumed that 50% of the incident magnetosheath ion population was transmitted through the RD (i.e. $t = NA/N_{sh} = 0.5$) and 50% was reflected back into the magnetosheath. This value is a rough accord with the values of t determined experimentally by *Fuselier et al.* [1992], although other studies have implied that this factor may be lower [Onsager et al., 1994; Lockwood et al., 1994]. Using a transmission factor t of 0.5 and the fitted density for the transmitted Cowley-D distribution, $N = 1.3A \times 10^7$ m^{-3}, we obtain a sheath density of $N_{sh} = 2N = 2.6A \times 10^7$ m^{-3}. This, along with the fitted temperature of $T = 3.1 \times 10^6$ K, are reasonable sheath values for a location of the X-line quite close to the nose of the magnetosphere. In addition, from equation (4), we find that the Alfvén speed in the magnetosheath is $V_A = 186 \pm 50$ km s^{-1} and hence the magnetic field $B_{sh} = V_A (\mu_o m_i N_{sh})^{0.5} = 43$ nT for A = 1.

Lastly, application of conservation of mass and energy to the X-line , yields the equation

$$B_{sp}' + B_{sh}' = (V_{FX}^2 \, m \, \mu_o/2) \, [(N_{sh}/B_{sh}') + (N_{sp}/B_{sp}')] \qquad (7)$$

where B_{sp}' and B_{sh}' are the components of the magnetosphere and magnetosheath magnetic fields normal to the X-line and N_{sp} and N_{sh} are the corresponding plasma densities in the magnetosphere and magnetosheath inflow regions. Because $N_{sp} << N_{sh}$ and B_{sp}' is generally greater than B_{sh}', we can neglect the (N_{sp}/B_{sp}') term in (7) to a first order approximation. This yields a quadratic equation for B_{sh}, taking the positive solution for which yields

$$\Delta B \approx B_{sh}' + B_{sp}' = [(B_{sp}'^2/4) + (V_{FX}^2\, m\, \mu_o\, N_{sh}/2)]^{1/2} \qquad (8)$$

Lockwood et al. [1994] have used this equation, along with simultaneous satellite data from the cusp and from the interplanetary medium, to estimate the magnetic shear across the X-line and the transmission factor, t. Their analysis assumes that the dayside magnetopause is in quasi-equilibrium and uses the pressure balance equation in order to relate the observed solar wind dynamic pressure to the internal magnetospheric field, B_{sp}. Unfortunately, for the data discussed in the present paper, the IMP-8 satellite was in an ideal location, but not tracked. Hence the analysis of *Lockwood et al.* [1994] cannot be repeated in full here. Nevertheless, their analysis should be possible with a large number of passes which do have simultaneous IMF or magnetosheath data and which display the feature in the cusp ion dispersion signature at A, as demonstrated in figure 1.

DISCUSSION AND CONCLUSIONS

We have analysed in detail a cusp ion step which was observed by DMSP-F10 on the equatorward edge of a poleward-moving event in the cusp region by the EISCAT radar. The combined observations are consistent with both being caused by pulsed reconnection, taking place at a location on the dayside magnetopause, as predicted by the pulsating cusp theory of *Lockwood and Smith* [1989]; *Cowley et al.* [1991] and *Smith et al.* [1992].

The pulsating cusp theory predicts cusp ion steps, but as mentioned in the introduction, steps can also be produced by spatial variations of the reconnection rate [*Onsager et al.*, 1994; *Weiss et al.*, 1994]. *Lockwood* [1994b] and *Lockwood and Smith* [1994] have discussed how the plasma flow must be parallel to the step on both sides and hence a rotation of the flow across the step reveals that it is temporal and not spatial in origin. The flow vectors in figure 4 reveal a small but persistent rotation towards northward with increasing latitude across the equatorward boundary of the second event, where the step discussed in this paper was observed. As discussed by *Lockwood* [1994b], such a rotation eliminates a spatial cause of this particular step.

Secondly, the pulsating cusp model predicts that the cusp will be one of a series of poleward-moving events [*Lockwood et al.*, 1993b; *Lockwood*, 1994a; b], as is found to be the case in these data. Not only does this not fit with a spatial origin of the step, but it also supports the concepts of ionospheric flow excitation put forward by *Cowley and Lockwood* [1992] on which the prediction of cusp ions steps by *Cowley et al.* [1991] and *Smith et al.* [1992] was based. Note that no other model of the ionospheric effects of flux transfer events (here meaning magnetopause reconnection pulses) can explain cusp ion steps, as it is the only model in which each region of newly-opened flux is appended directly equatorward of its predecessor. The concepts of flow excitation in these models are also supported by the relatively constant poleward flow observed by EISCAT during these events (V_N being roughly 500 m s^{-1}) at these times. This is because induction effects mean that the reconnection pulses cause the open/closed boundary to migrate equatorward, rather than exciting poleward flow [*Lockwood et al.*, 1993b]. The poleward flow is inductively smoothed with a time constant, which is estimated to be near 20 min. and which is therefore considerably greater than the 4 min. between the events discussed here [*Lockwood*, 1994a]. The equatorward motions of the open/closed boundary can be seen in the behaviour of the enhanced T_e events, with each event forming equatorward of the one before, reflecting the equatorward erosion of the boundary during the reconnection pulse which gives rise to the event.

The uncertainties in determining the time-of-flight low-energy cut-off of the cusp/cleft ions mean that it is difficult to estimate the exact distance from the satellite to the reconnection site. However, we can state from inspection of the velocity distribution functions at any one time that a minimum value is $6R_E$ and a maximum value is $38R_E$, which place the reconnection site somewhere on the dayside magnetopause. The first-order estimate of 16 R_E deduced by *Lockwood et al.* [1993a] falls within the deduced range for d, but the value of $100R_E$ deduced by *Newell and Meng* [1994] does not. There are three causes of this. The first is that *Newell and Meng* followed *Lockwood et al.* in using their rough estimate based on the average repeat period between the events (5.3 min), rather than the interval between the two events in question, which we here show to be just over 4 min (figure 4). Secondly *Newell and Meng* estimate the cut-off using the differential energy flux spectra and define the a cut-off using the peak of this spectrum. We have here shown that the peak of the spectrum bears a complex and variable relation to the low-energy cut-off and that definitions which place the cut-off in fixed relation to the peak will be misleading. Lastly, *Newell and Meng* associate only the steepest part of the step with the period of low-reconnection between the pulses. However, the full evaluation of the reconnection rate using the method of *Lockwood and Smith* [1992] (figures 8 and 9) shows

that, at low energies, a low reconnection rate gives only a small gradient to the cut off. Therefore in restricting the step to the steepest part *Newell and Meng* underestimate the length of the period of low reconnection rate. All three of these factors act to increase the distance estimate of *Newell and Meng*. Our analysis does not support their conclusion that the pulsating cusp model is incorrect because it predicts a reconnection site which is not on the dayside magnetopause.

Indeed, using the time series of the distribution function at each energy level of the instrument has here provided us with a much more detailed view of the behaviour of this cut-off as a function of time, and this gives the distance from the satellite to the X-line to be $13R_E$. This implies that the reconnection is quite close to the subsolar point for these equinox conditions (for example the subsolar point is at a distance of $14R_E$ using the Tsyganenko T89 model for equinox and Kp of 6 [*Lockwood and Smith*, 1994]). A near subsolar location of the reconnection X-line is consistent with the deduced value of the field-aligned sheath flow speed near the X-line, which is only 13±85 km s^{-1}. This strongly supports the low-latitude location of the X-line inferred from magnetopause measurements [*Daly et al.*, 1984; *Paschmann*, 1984; *Gosling et al.*, 1990a; *Rijnbeek et al.*, 1984] and from mid-altitude cusp ion dispersion signatures [*Phillips et al.*, 1993; *Lockwood and Smith*, 1994] and low-altitude cusp dispersion signatures [*Reiff et al.*, 1977; *Carlson and Torbert*; 1980]. Note that previous studies of the distance to the X-line from low-altitude cusp data have employed the observed convection velocity in the Earth's frame and hence assumed steady-state conditions, such that the ionospheric projection of the X-line is static. The method employed here is based on time elapsed since reconnection and does not make any such assumption.

The accurate determination of the low cut-off energy allows the field-parallel part of the Cowley-D distribution injected near the X-line to be determined, using Loiuville's theorem (figure 11). This allows a wealth of information about the conditions at the reconnection site to be estimated. These include the ion temperature, density, magnetic field and field-aligned magnetosheath flow in the magnetosheath, in the vicinity of the X-line. Using solar wind values the magnetic shear across the X-line, and the ion transmission factor across the magnetopause RD could also be estimated [*Lockwood et al.*, 1994]. In addition, the reconnection rate is computed using the method of *Lockwood and Smith* [1992].

The finding that the field-aligned magnetosheath flow is near zero at the X-line is interesting as that was also the case in the quasi-steady cusp pass studied, using the same techniques, by *Lockwood et al.* [1994]. Work is underway to apply the methods described here to the large number of cusp passes which reveal the required feature between

A and B in figure 1. Hence the method presented here opens up exciting new possibilities for studies of the causes and behaviour of magnetopause reconnection.

Acknowledgements. We thank the director and staff of the EISCAT Scientific Association for their assistance. EISCAT is supported by the research councils of France, Germany, Sweden, Norway and the UK.

REFERENCES

Aggson, T.L., et al., Electric field measurements at the magnetopause: 1. Observations of large convective velocities at rotational magnetopause discontinuities, *J. Geophys. Res.*, ***88***, 10000, 1983.

Brace, L.H., et al., A global view of the F-region electron density and temperature, *Geophys. Res. Lett.*, *9*, 989, 1982.

Carlson, C.W. and R.B. Torbert, Solar wind injections in the morning auroral oval, *J. Geophys. Res.*, *85*, 2903-2908, 1980.

Curtis, S.A. et al., DE-2 cusp observations:role of plasma instabilities in topside ionospheric heating and density fluctuations, *Geophys. Res. Lett.*, *9*, 997, 1982.

Cowley, S.W.H., The causes of convection in the Earth's magnetosphere: A review of developments during IMS, *Rev. Geophys.*, *20*, 531, 1982.

Cowley, S.W.H and M. Lockwood, Excitation and decay of solar-wind driven flows in the magnetosphere-ionosphere system, *Annales Geophys.*, *10*, 103-115, 1992.

Cowley, S.W.H and C.J. Owen, A simple illustrative model of open flux tube motion over the dayside magnetopause, *Planet. Space Sci.*, *37*, 1461, 1989.

Cowley, S.W.H., et al., The ionospheric signature of flux transfer events, in *"CLUSTER - dayside polar cusp", ESA SP-330,* editor C.I Barron. European Space Agency Publications, The Netherlands, pp 105-112, 1991.

Daly, P. W., et al., The distribution of reconnection geometry in flux transfer events using energetic plasma and magnetic data, *J. Geophys. Res.* ,*89*, 3843, 1984.

Escoubet, C.P., et al., Staircase ion signature in the polar cusp: a case

study, *Geophys. Res. Lett., 19,* 1735, 1992.

Fasel, G.J., Poleward-Moving auroral forms: a statistical study, *J. Geophys. Res.,* submitted, 1994.

Fuselier, S.A., et al., Ion reflection and transmission during reconnection at the Earth's subsolar magnetopause, *Geophys. Res. Lett., 18,* 139, 1991.

Gosling, J.T., et al., Plasma flow reversals at the dayside magnetopause and the origin of asymmetric polar cap convection, *J. Geophys. Res., 95,* 8073, 1990a.

Gosling, J.T., et al., Cold ion beams in the low-latitude boundary layer during accelerated flow events, *Geophys. Res. Lett., 17,* 2245, 1990b.

Gosling, J.T., et al., The electron edge of the low-latitude boundary layer during accelerated flow events, *Geophys. Res. Lett., 17,* 1833, 1990c.

Hill, T.W. and P.H. Reiff, Evidence of magnetospheric cusp proton acceleration by magnetic merging at the dayside magnetopause, *J. Geophys. Res., 82,* 3623-3628, 1977.

Lockwood, M., Ionospheric signatures of pulsed magnetopause reconnection *in "Physical signatures of magnetopause boundary layer Processes"*, ed. J. Holtet and A. Egeland, NATO ASI Series C425, Kluwar, 229-243, 1994a.

Lockwood, M., Ground-Based and Satellite Observations of the Cusp: Evidence for Pulsed Magnetopause Reconnection, in *"Physics of the Magnetopause"*, ed. B.U.O Sonnerup, Proc. Chapman Conference, San Diego, 1994, AGU Monograph, in press, 1994b.

Lockwood, M. and M.F. Smith, Low altitude signatures of the cusp and flux transfer events, *Geophys. Res. Lett., 16,* 879, 1989.

Lockwood, M. and M.F. Smith, Reply to Newell, *Geophys. Res. Lett., 17,* 305, 1990.

Lockwood, M., and M.F. Smith, The variation of reconnection rate at the dayside magnetopause and cusp ion precipitation, *J. Geophys. Res., 97,* 14,841, 1992.

Lockwood, M. and M.F. Smith, Comment on "Mapping the dayside ionosphere to the magnetosphere according to particle precipitation characteristics" by Newell and Meng, *Geophys. Res. Lett., 20,* 1739,

Lockwood, M. and M.F. Smith, Low- and mid-altitude cusp particle signatures for general magnetopause reconnection rate variations:I. Theory, *J.Geophys.Res., 99,* 8531, 1994.

Lockwood, M. and M.N. Wild, On the quasi-periodic nature of magnetopause FTEs, *J. Geophys. Res., 98,* 5935, 1993.

Lockwood, M, et al., Ionospheric signatures of pulsed magnetic reconnection at the Earth's magnetopause, *Nature, 361 (6411),* 424, 1993a.

Lockwood, M., et al., Variability of dayside convection and motions of the cusp/cleft aurora, *Geophys. Res. Lett., 20,* 1011, 1993b.

Lockwood, M., et al., The characteristics of the magnetopause reconnection X-line deduced from low-altitude satellite observations of cusp ions, *Geophys. Res. Lett.*, submitted, 1994.

Newell, P. T. and C.-I. Meng, The cusp and the cleft/LLBL: Low altitude identification and statistical local time variation, *J. Geophys. Res., 93,* 14,549, 1988.

Newell, P. T. and C. I. Meng, Ion acceleration at the equatorward edge of the cusp: low altitude observations of patchy merging, *Geophys. Res. Lett, 18,* 1829-1832, 1991.

Newell, P.T. and C.-I. Meng, Mapping the dayside ionosphere to the magnetosphere according to particle precipitation characteristics, *Geophys. Res. Lett., **19,*** 609-612, 1992.

Newell, P.T. and C.-I. Meng, Reply, *Geophys. Res. Lett., 20,* 1741, 1993.

Newell, P.T. and C.-I. Meng, Magnetopause dynamics as inferred from plasma observations on low-altitude satellites, in *"Physics of the Magnetopause"*, ed. B.U.O Sonnerup, Proc. Chapman Conference, San Diego, 1994, AGU Monograph, in press, 1994.

Newell, P.T., et al., Identification an observation of the plasma mantle at low altitude, *J.Geophys.Res., 96,* 3545, 1991

Onsager, T.G., et al., Model of magnetosheath plasma in the magnetosphere: cusp and mantle precipitations at low altitudes, *Geophys. Res. Lett., 20,* 479, 1993.

Onsager, T.G., et al., Low altitude observations and modelling of quasi-steady magnetopause reconnection, *J. Geophys. Res.*, in press, 1994.

Paschmann, G., The Earth's magnetopause, in *Achievements of the international magnetospheric study, IMS*, pp 53-64, ESA SP-217, ESTEC, Nordvijk, The Netherlands, 1984.

Paschmann, G., et al., Plasma acceleration at the Earth's magnetopause: Evidence for reconnection, *Nature, 282,* 243, 1979.

Paschmann, G., et al., The magnetopause for large magnetic shear: AMPTE/IRM observations, *J. Geophys. Res., 91,* 11099, 1986.

Phillips, J.L., et al., Well-resolved observations by ISEE 2 of ion dispersion in the magnetospheric cusp, *J. Geophys. Res., 98,* 13,429, 1993.

Reiff, P.H., T.W. Hill, and J.L. Burch, Solar wind plasma injection at the dayside magnetospheric cusp, *J. Geophys. Res., 82,* 479, 1977.

Rijnbeek, R. P., et al., A survey of dayside flux transfer events observed by the ISEE 1 and 2 magnetometers, *J. Geophys. Res., 89,* 786, 1984.

Rosenbauer, H., et al., HEOS-2 plasma observations in the distant polar magnetosphere: the plasma mantle, *J. Geophys. Res., 80,* 2723, 1975.

Sanchez, E.R. and G.L. Siscoe, IMP 8 magnetotail boundary crossings: a test of the MHD models for an open magnetosphere, *J. Geophys. Res., 95,* 20771, 1990.

Sanchez, E.R., et al., Observations of rotational discontinuity-slow mode expansion fan structure of the magnetotail boundary, *J. Geophys. Res., 95,* 61, 1990.

Shelley, E.G., R.D. Sharp, and R.G. Johnstone, He^{++} and H^{+} flux measurements in the dayside cusp: estimates of convection electric field, *J. Geophys. Res., 81,* 2363-2370, 1976.

Smith, M.F. and Rodgers, D.J., Ion distributions at the dayside magnetopause, *J. Geophys. Res., 95,* 11,617, 1991.

Smith, M.F., et al., The statistical cusp: a simple flux transfer event model, *Planet. Space Sci., 40,* 1251, 1992.

Sonnerup, B.U.Ö., et al., Evidence for magnetic field reconnection at the Earth's magnetopause, *J. Geophys. Res., 86,* 10049, 1990.

Sonnerup, B.U.Ö., et al., The magnetopause for large magnetic shear: analysis of convection electric fields from AMPTE/IRM, *J. Geophys. Res., 95,* 10,541, 1990.

Titheridge, J.E., Ionospheric heating beneath the magnetospheric cleft, *J. Geophys. Res., 81,* 1976.

Waterman, J., et al., Ionospheric footprint of magnetosheathlike particle precipitation observed by an incoherent scatter radar, *J. Geophys. Res., 99,* 3855, 1994.

Weiss, L.A., et al., Flow-aligned jets in the magnetospheric cusp: results from the GEM pilot programme, *J. Geophys. Res.,* submitted, 1994.

Wickwar, V.B. and W. Kofman, Dayside auroras at very high latitudes: the importance of thermal excitation, *Geophys. Res. Lett., 11,* 923-926, 1984.

Wickwar, V.B., et al., The 6300Å $O(^1D)$ airglow and dissociative recombination, *Planet. Space Sci., 22,* 709-724, 1974.

C.J. Davis and M. Lockwood, Rutherford Appleton Laboratory, Chilton, Didcot, OX11 0QX, UK. (e-mail: Internet. mike@eiscat.ag.rl.ac.uk)

W.F. Denig, Phillips Laboratory, PL/GPSG, Hanscom AFB, Bedford, MA01731-5000, USA.

M. F. Smith, Laboratory for Extraterrestrial Physics, NASA Goddard Space Flight Center, Greenbelt, MD 20771. (e-mail: Internet. smith@lepmfs.gsfc.nasa.gov)

T.G. Onsager, Institute for the Study of the Earth, Oceans, and Space and Department of Physics, University of New Hampshire, Durham, NH 03824, USA

Legends to figures.

Fig. 1. Schematic of cusp ion precipitation observed by an equatorward-moving satellite for poleward convection (southward IMF). The lower solid line shows the minimum detectable energy, E_{ic}, as a function of observation time t_s. The dashed lines 1,2, 3 and 4 connect ions injected at the same time (t_1, t_2, t_3 and t_4, respectively) and point (P_1, P_2, P_3 and P_4) at the magnetopause where $t_4 > t_3 > t_2 > t_1$. The dotted vertical lines are typical boundaries of the cleft, cusp and mantle regions defined from the spectral characteristics at any on t_s. In this figure the X-line is at P_1 from which the field lines evolve along the magnetopause at a de-Hoffman Teller velocity of V_{FX}.

Fig. 2. The evolution of a newly-opened field line from a dayside magnetopause X-line, X, to the tail lobe. Ions injected across the magnetopause while the field line is in the four positions marked 1 to 4 are spread along the corresponding dashed lines in figure 1. The satellite, S, is shown making observations on a field line in position 4, in the northern hemisphere topside ionosphere, a distance d from the X-line.

Fig. 3. Field-parallel segments of the Cowley-D ion distribution functions in the open LLBL, injected across the magnetopause when the field line is in positions 1-4 shown on figure 2. These distributions are dispersed along the corresponding dashed lines in figure 1. The dashed line joining the solid circles is the spectrum seen at low altitudes at a time t_s, when the satellite is in the region classed as cleft in figure 1: the dotted line joining the squares is an example of that seen when S is in the "cusp" region.

Fig. 4. Detail of the poleward-moving events seen by the EISCAT UHF radar on 28 March 1992, as reported by *Lockwood et al.* [1993a]. The grey scale gives the temperature of the ambient ionospheric electron gas and the arrows mark the location where the DMSP-F10 satellite observed upward steps in the ion dispersion signature on the edges of the "cusp" precipitation. The flow vectors are derived by combining the line-of-sight velocities seen simultaneously by the VHF and UHF radars.

Fig. 5. Variation of estimates of the lower cut-off energy, E_{ic}, as a function of observation time t_s. The dotted and the dot-dash lines are, respectively, the one-count level, E_1, and the peak of the distribution function, E_p, derived from figure 6. The solid line is the mean of the two $[E_{ic}]_E$. The horizontal bars are the times of the decay in $f(t_s)$ for each energy channel, derived from figure 7, the centre of each being marked by an open circle. The dashed line joins the one-second

values, $[E_{ic}]_T$, which give a best fit to the open circles.

Fig. 6. Sequential ion distribution functions f(E) from DMSP-F10 on 28 March 1992: (a). 10:11:14-10:11:17 (t_s of 194-197, where t_s is defined to be zero at 10:08:00); (b). 10:11:17-10:11:20 (t_s = 197-200); and (c). 10:11:20 - 10:11:23 (t_s = 200 - 203). All plots use logarithmic E and f scales.

Fig. 7. Time series of distribution function $f(t_s)$ for each energy channel: (a) E of 140eV - 66eV ; (b) 440eV - 140eV; (c) 1.38 keV - 0.44 keV and (d) 4.4keV - 1.38keV. Note in (a) the t_s axis is shifted by 6 s relative to (b)-(d) to reveal a fall in f at t_s = 184-187 s.

Fig. 8. Variation of reconnection rate, ε_y, for an assumed distance from the satellite to the X-line, d, of $16R_E$ and using $E_{ic} = [E_{ic}]_E$ (solid line) and $E_{ic} = [E_{ic}]_T$ (dashed line).

Fig. 9. Variation of reconnection rate ε_y for d = 8 R_E (solid line) and d = 22 R_E (dot-dash line) using $E_{ic} = [E_{ic}]_E$.

Fig. 10. The delay between the reconnection pulse and the onset of the associated event seen by EISCAT, as a function of the assumed distance to the X-line, d. Estimates for E_{ic} used are: E_l (dotted lines); $[E_{ic}]_T$ (dashed lines); $[E_{ic}]_E$ (solid lines) and E_p (dot-dash lines). The lines are in pairs, the steeper of the pair being for the first event/reconnection pulse, the other being for the second. The intersection point of each pair gives the distance d.

Fig. 11. The Cowley-D distribution function in the (open) LLBL close to the reconnection X-line. The open circles are the values of $f(E_{ic})$, taken from the last integration point before the fall in $f(t_s)$ shown in figure 5. The crosses are $f(E_p)$ for those distribution functions where E_l and E_p are only one energy channel apart. The solid line is the one-count level. The dot-dash line is the best least-squares fit to these data points for a truncated drifting Maxwellian of field-parallel temperature T = 3.1 x 10^6 K, "one dimensional" density N = 1.3 x 10^7 m^{-3} and field-aligned bulk velocity 385 km s^{-1}. The low-velocity cut-off of the D is placed at 206 eV (equivalent to 199 km s^{-1}).

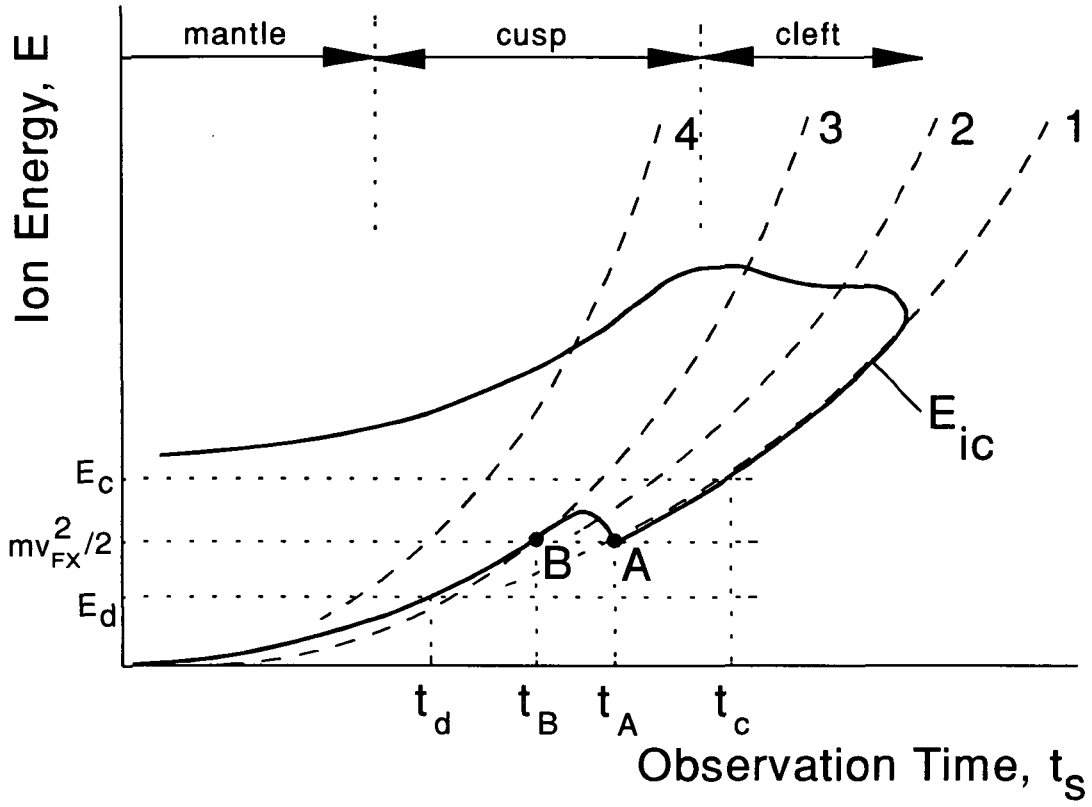
mantle
cusp
cleft
Ion Energy, E
4
3
2
1
E_{ic}
E_c
$mv_{FX}^2/2$
E_d
B
A
t_d
t_B
t_A
t_c
Observation Time, t_s

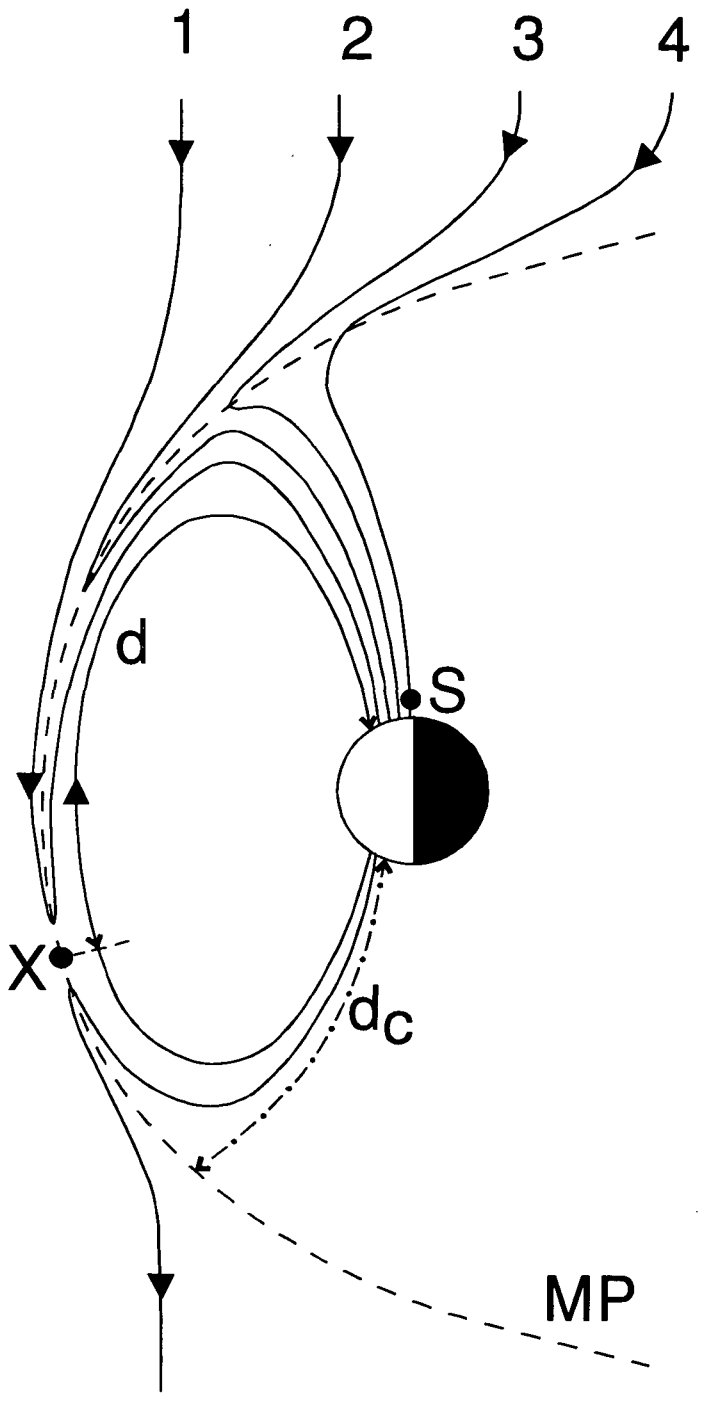

2

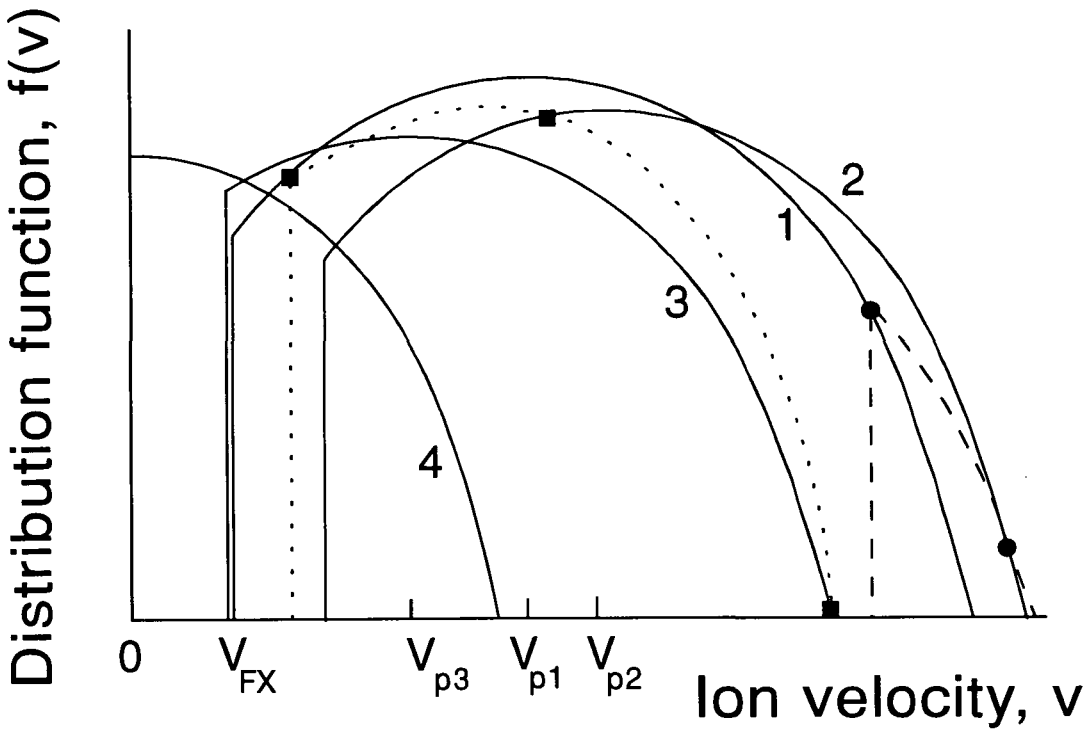
Distribution function, f(v)
0
V_{FX}
V_{p3}
V_{p1}
V_{p2}
Ion velocity, v
1
2
3
4

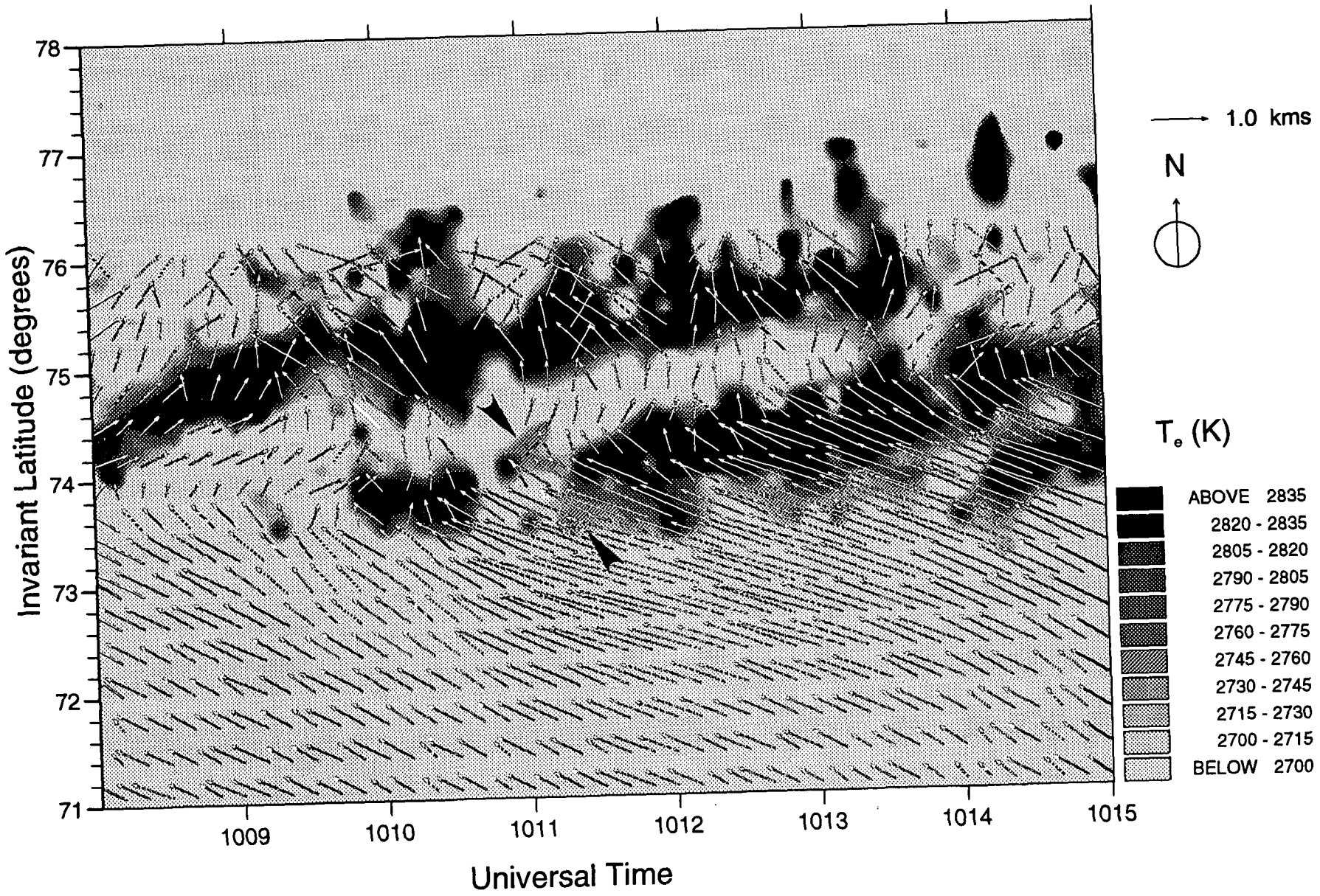
Experiment : SP-UK-CONV UHF Azimuth 344.8 Degrees
Time Interval : 10:08:00 28 March 1992 - 10:15:00 28 March 1992
Invariant Latitude (degrees)
78
77
76
75
74
73
72
71
1009
1010
1011
1012
1013
1014
1015
Universal Time
1.0 kms
N
T_e (K)
ABOVE 2835
2820 - 2835
2805 - 2820
2790 - 2805
2775 - 2790
2760 - 2775
2745 - 2760
2730 - 2745
2715 - 2730
2700 - 2715
BELOW 2700

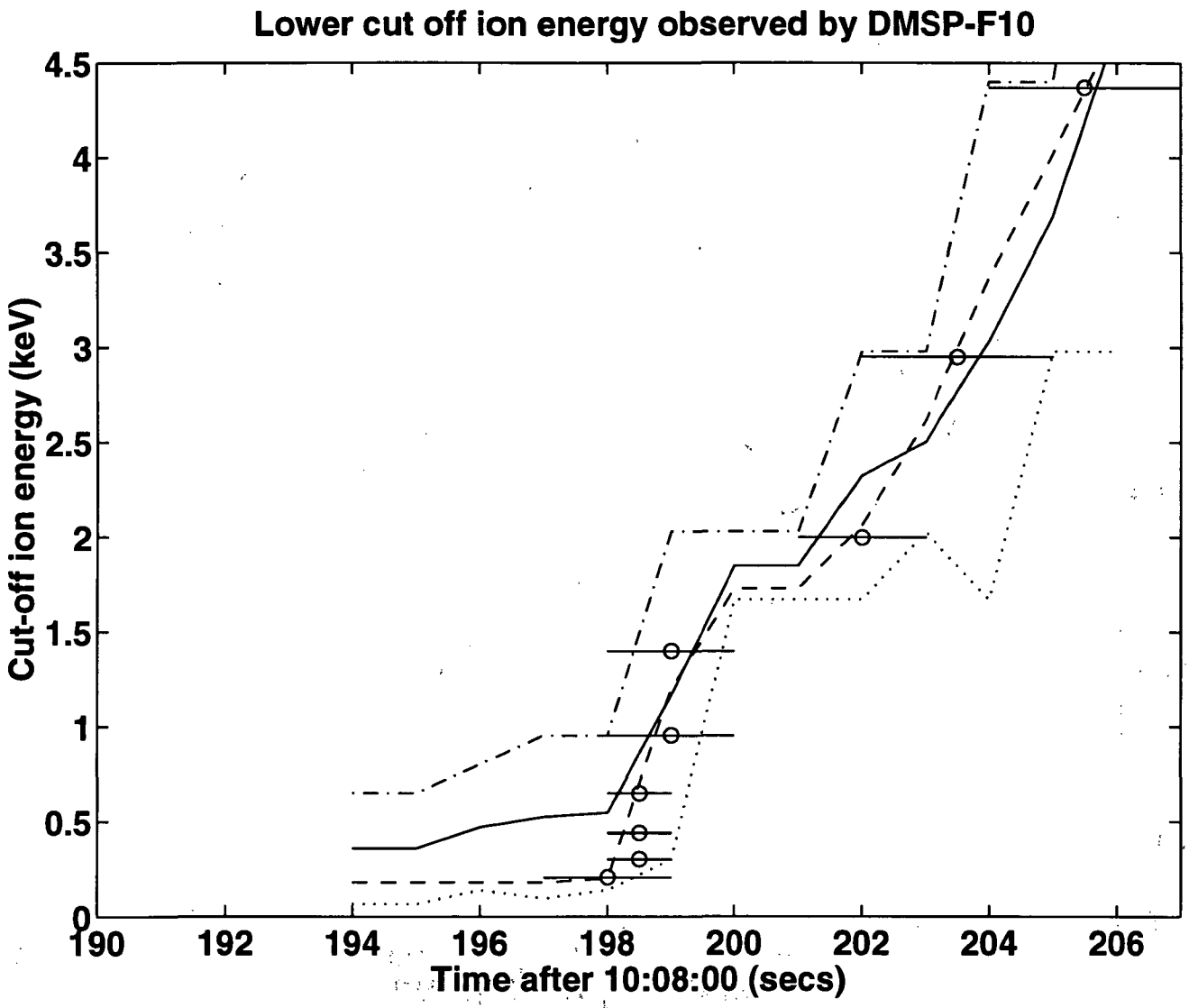
Lower cut off ion energy observed by DMSP-F10
Cut-off ion energy (keV)
Time after 10:08:00 (secs)
0
0.5
1
1.5
2
2.5
3
3.5
4
4.5
190
192
194
196
198
200
202
204
206

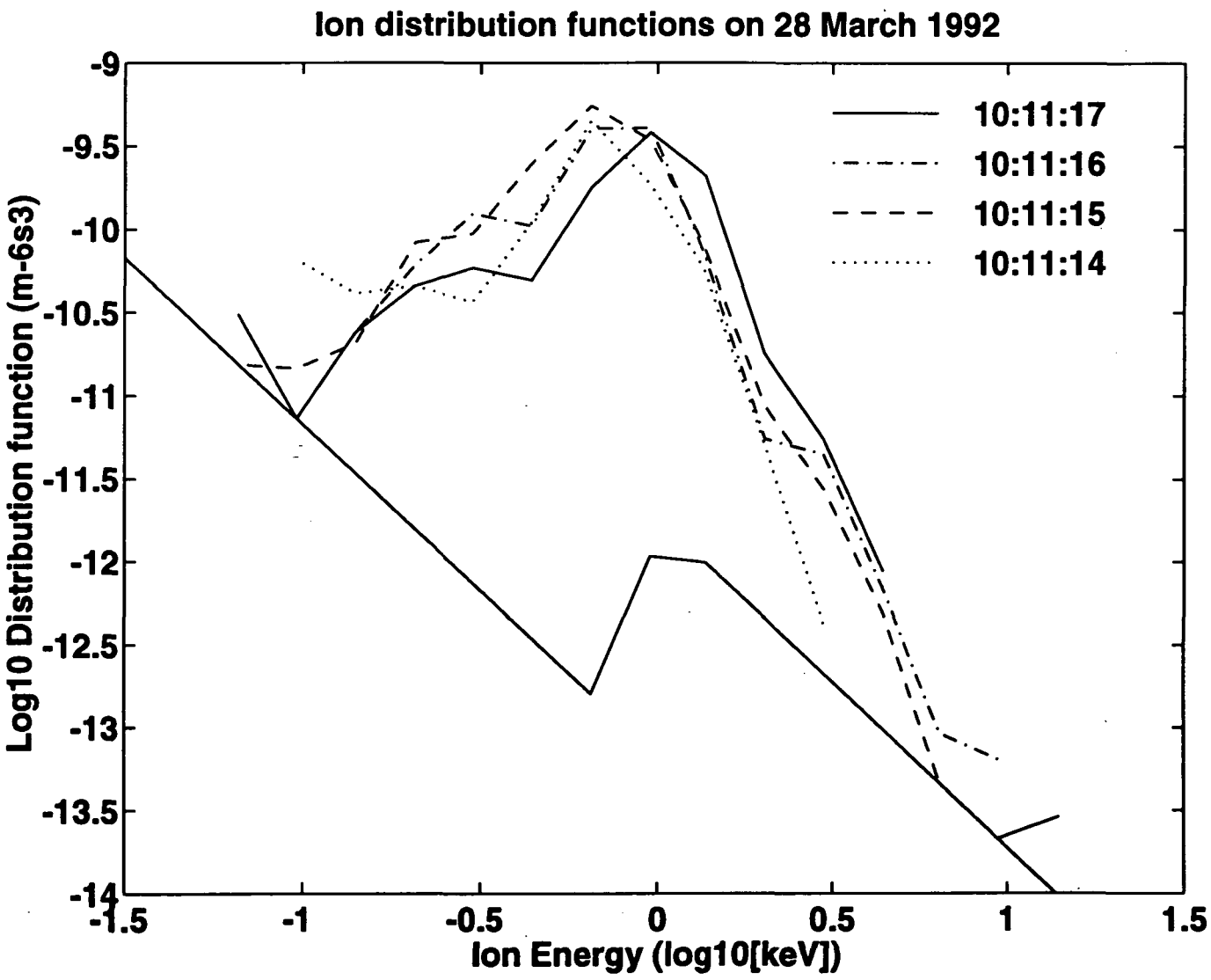
Ion distribution functions on 28 March 1992
Log10 Distribution function (m-6s3)
-9
-9.5
-10
-10.5
-11
-11.5
-12
-12.5
-13
-13.5
-14
-1.5
-1
-0.5
0
0.5
1
1.5
Ion Energy (log10[keV])
10:11:17
10:11:16
10:11:15
10:11:14

6a

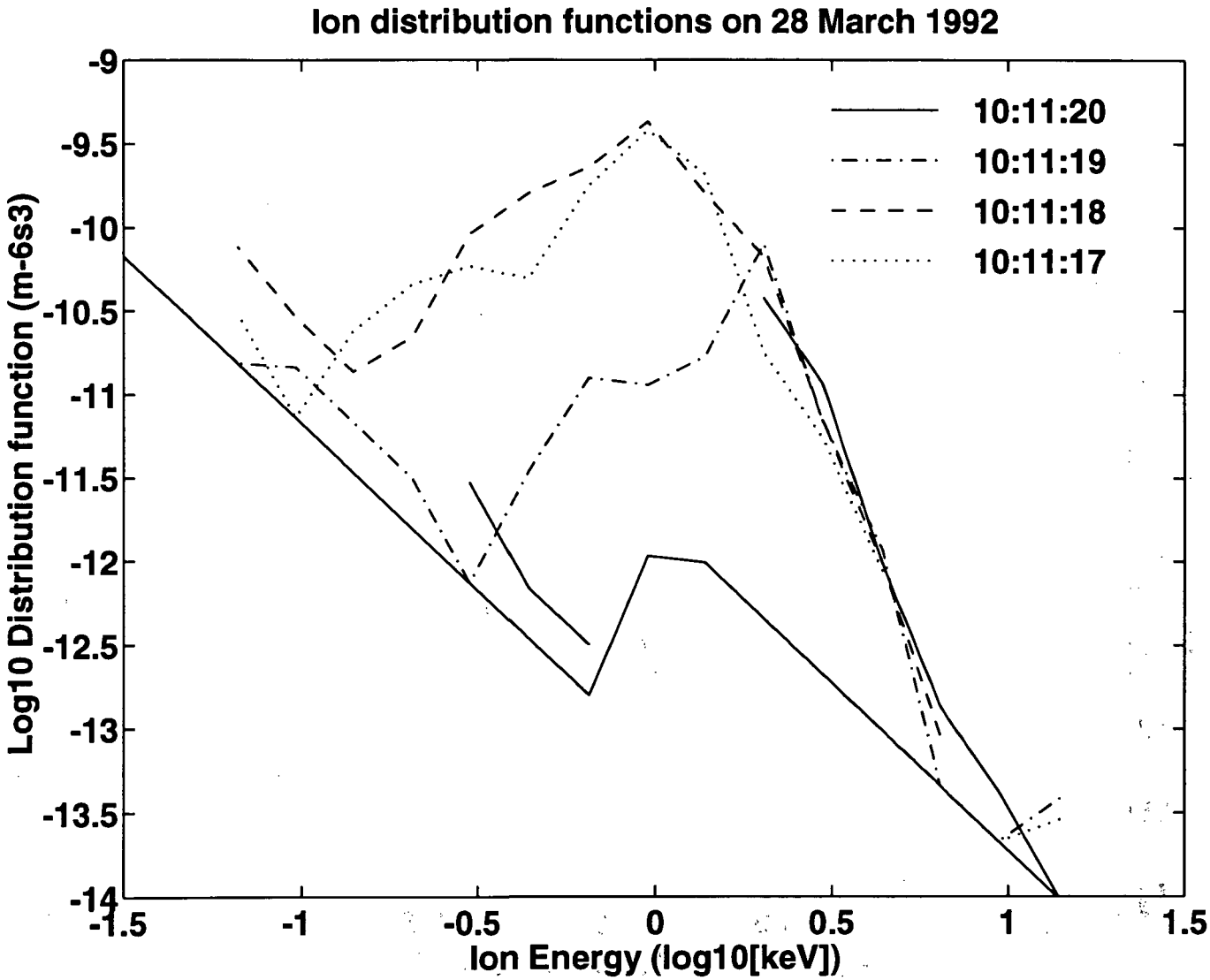
Ion distribution functions on 28 March 1992
Log10 Distribution function (m-6s3)
Ion Energy (log10[keV])
10:11:20
10:11:19
10:11:18
10:11:17
-9
-9.5
-10
-10.5
-11
-11.5
-12
-12.5
-13
-13.5
-14
-1.5
-1
-0.5
0
0.5
1
1.5

6b

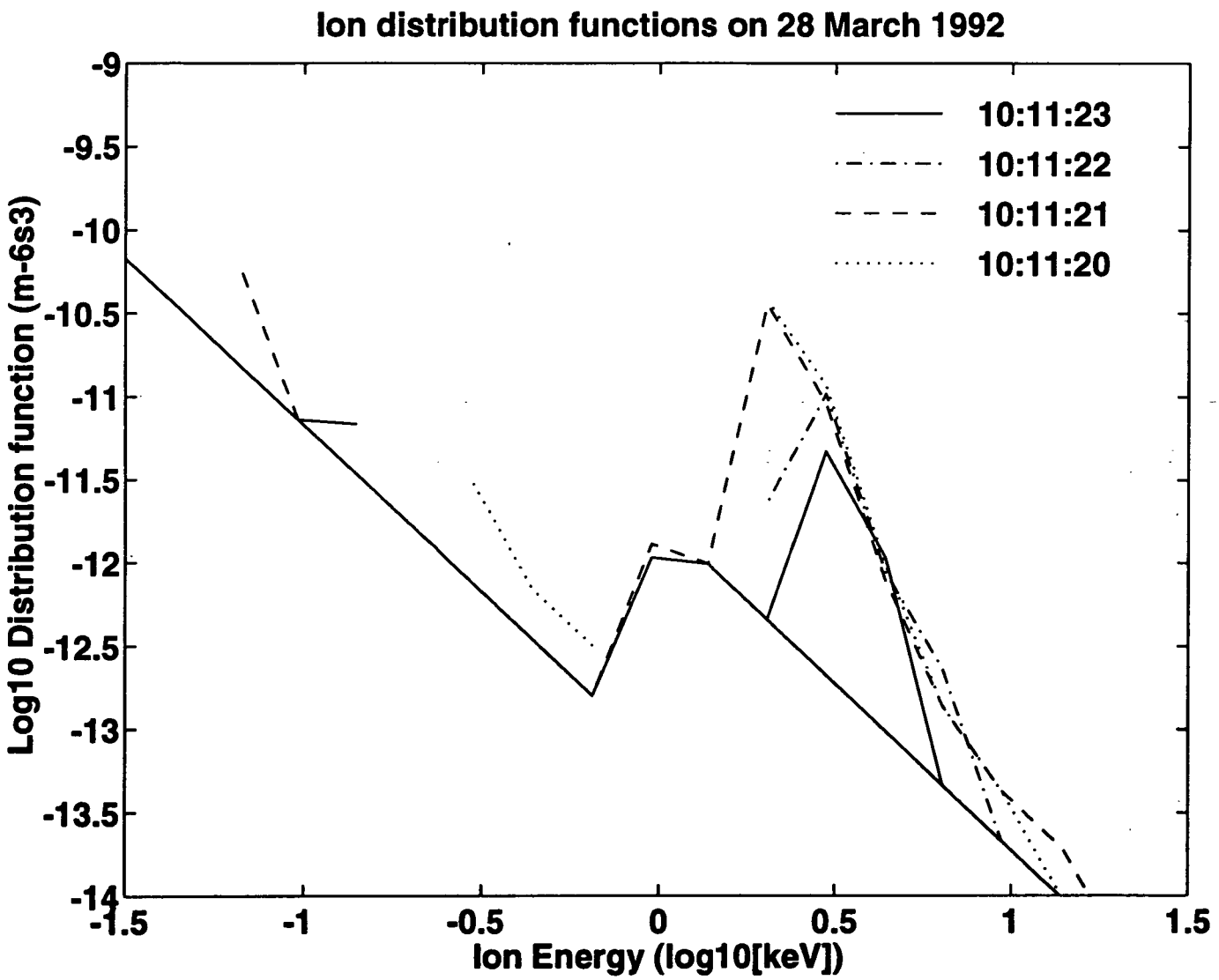
Ion distribution functions on 28 March 1992
10:11:23
10:11:22
10:11:21
10:11:20
Log10 Distribution function (m-6s3)
-9
-9.5
-10
-10.5
-11
-11.5
-12
-12.5
-13
-13.5
-14
-1.5
-1
-0.5
0
0.5
1
1.5
Ion Energy (log10[keV])

6c

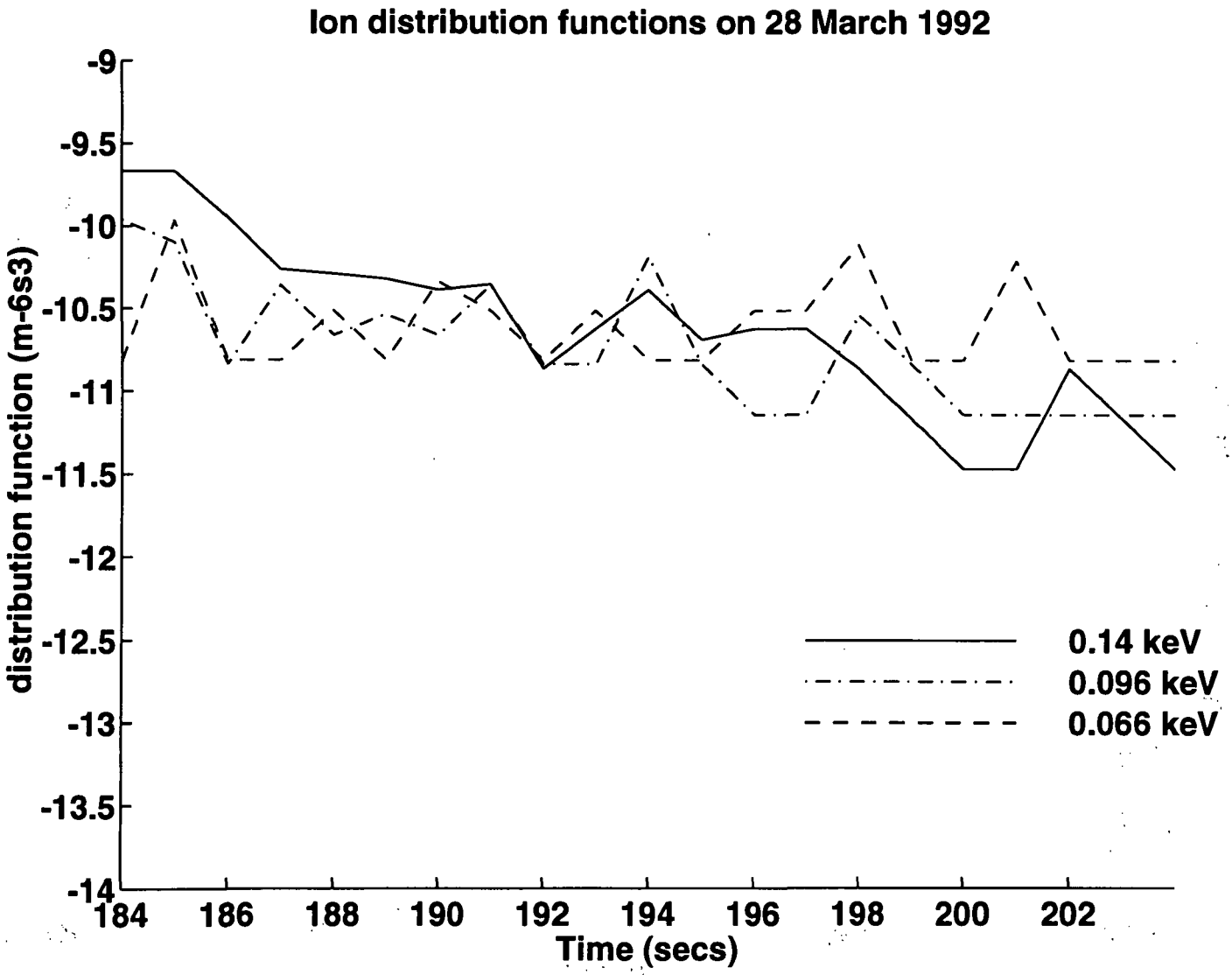
Ion distribution functions on 28 March 1992
distribution function (m-6s3)
-9
-9.5
-10
-10.5
-11
-11.5
-12
-12.5
-13
-13.5
-14
184
186
188
190
192
194
196
198
200
202
Time (secs)
0.14 keV
0.096 keV
0.066 keV

7a

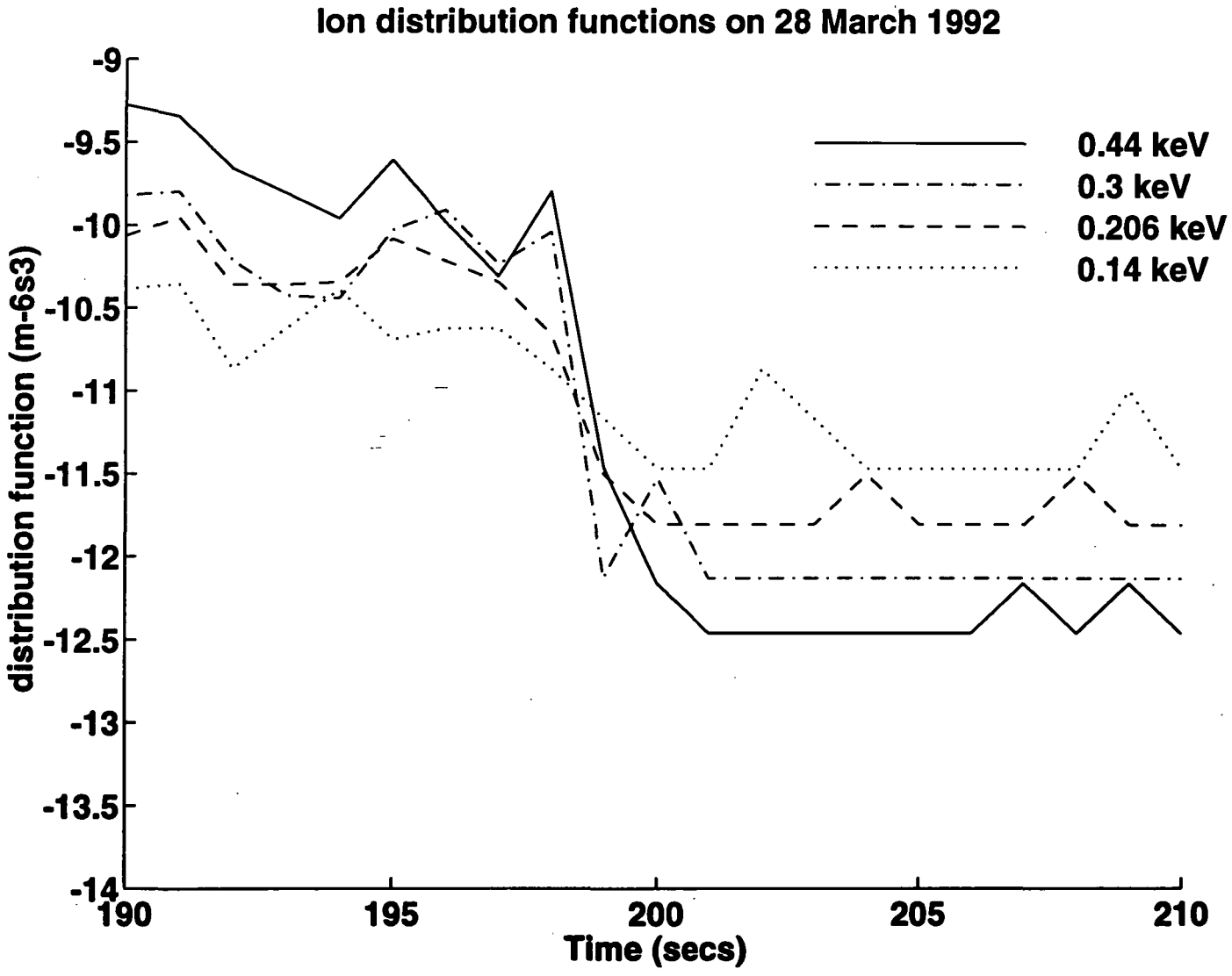
Ion distribution functions on 28 March 1992
-9
-9.5
-10
-10.5
-11
-11.5
-12
-12.5
-13
-13.5
-14
distribution function (m-6s3)
190
195
200
205
210
Time (secs)
0.44 keV
0.3 keV
0.206 keV
0.14 keV

7b

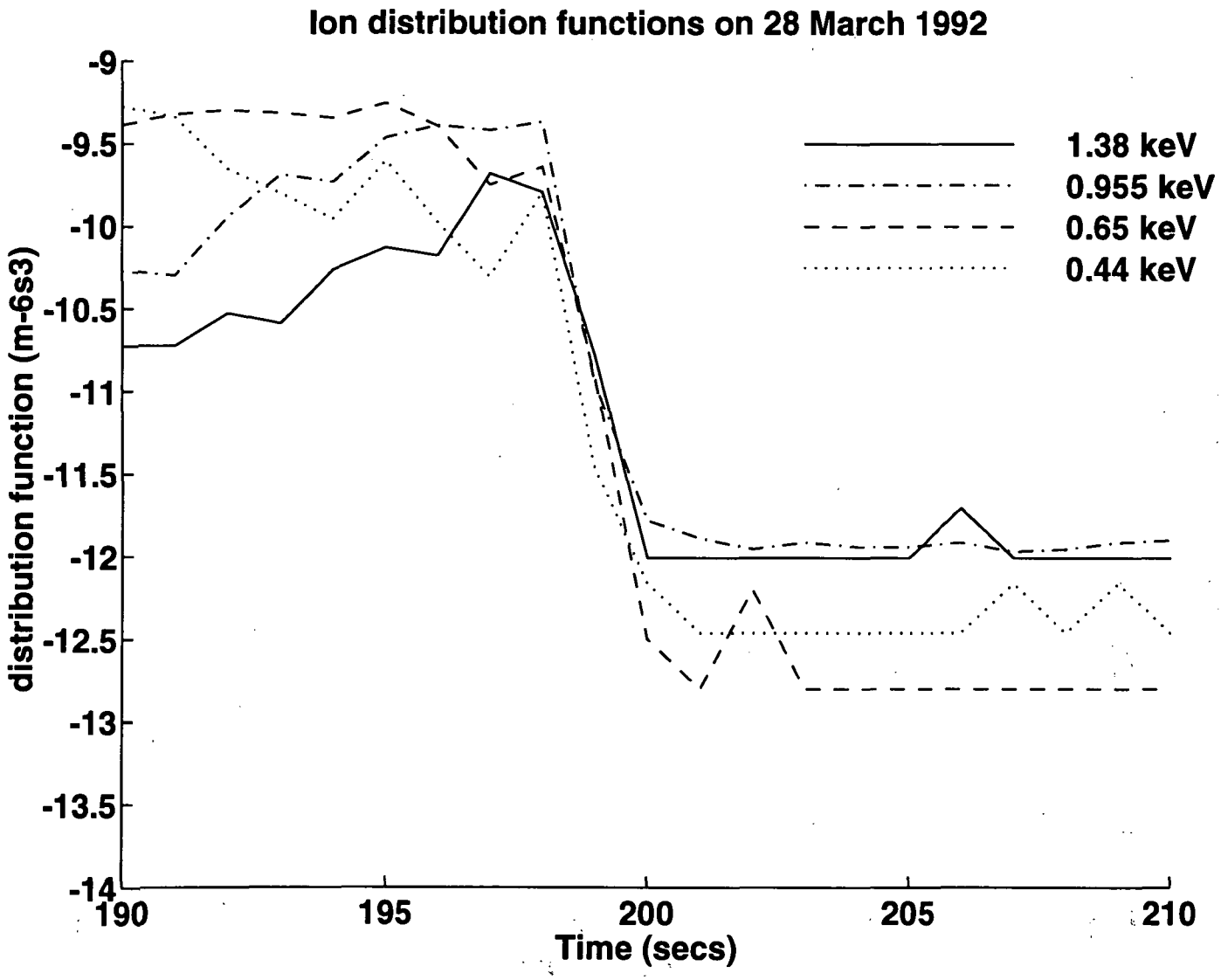
Ion distribution functions on 28 March 1992
distribution function (m-6s3)
-9
-9.5
-10
-10.5
-11
-11.5
-12
-12.5
-13
-13.5
-14
190
195
200
205
210
Time (secs)
1.38 keV
0.955 keV
0.65 keV
0.44 keV

7c

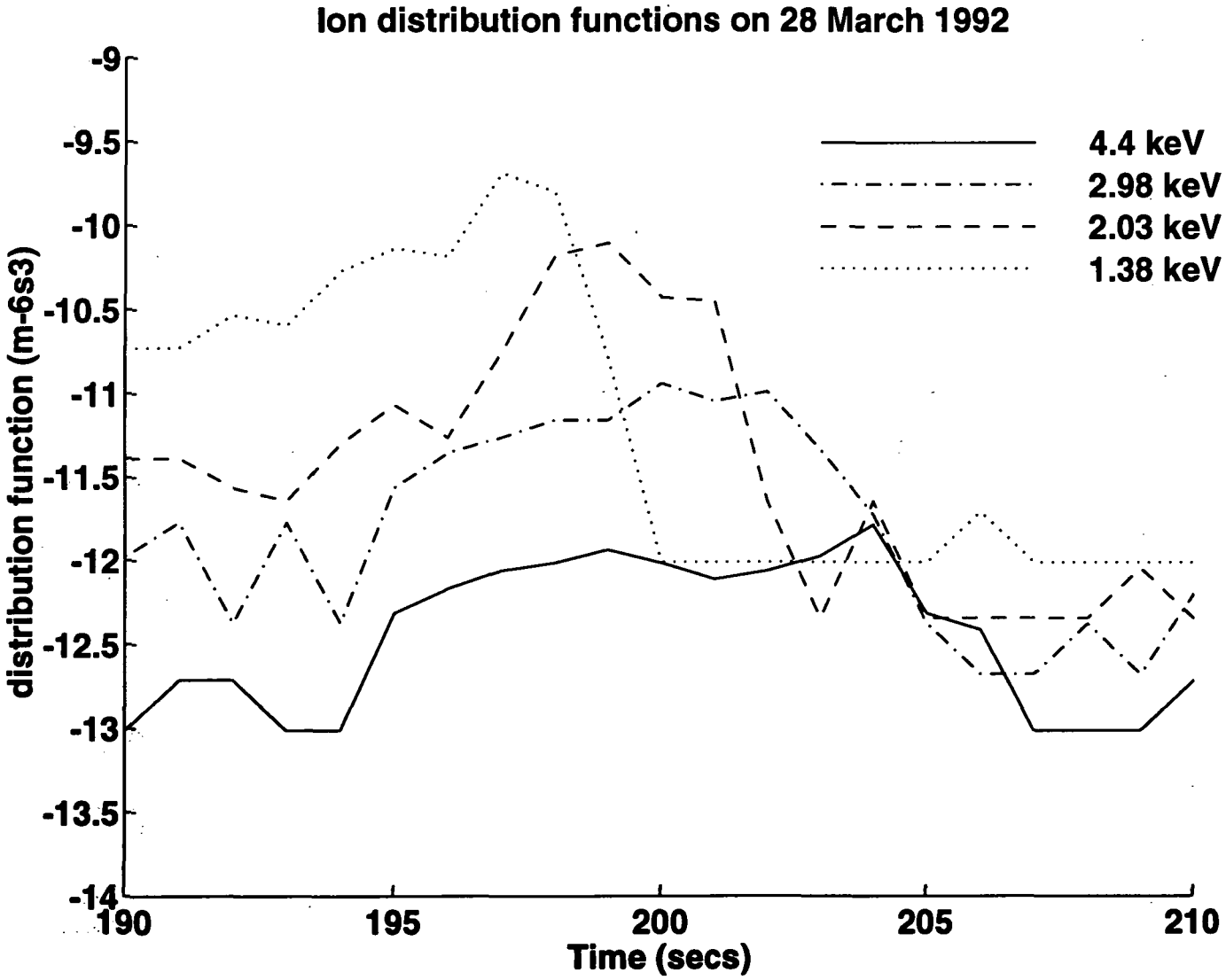
Ion distribution functions on 28 March 1992
-9
-9.5
-10
-10.5
-11
-11.5
-12
-12.5
-13
-13.5
-14
distribution function (m-6s3)
190
195
200
205
210
Time (secs)
4.4 keV
2.98 keV
2.03 keV
1.38 keV

7d

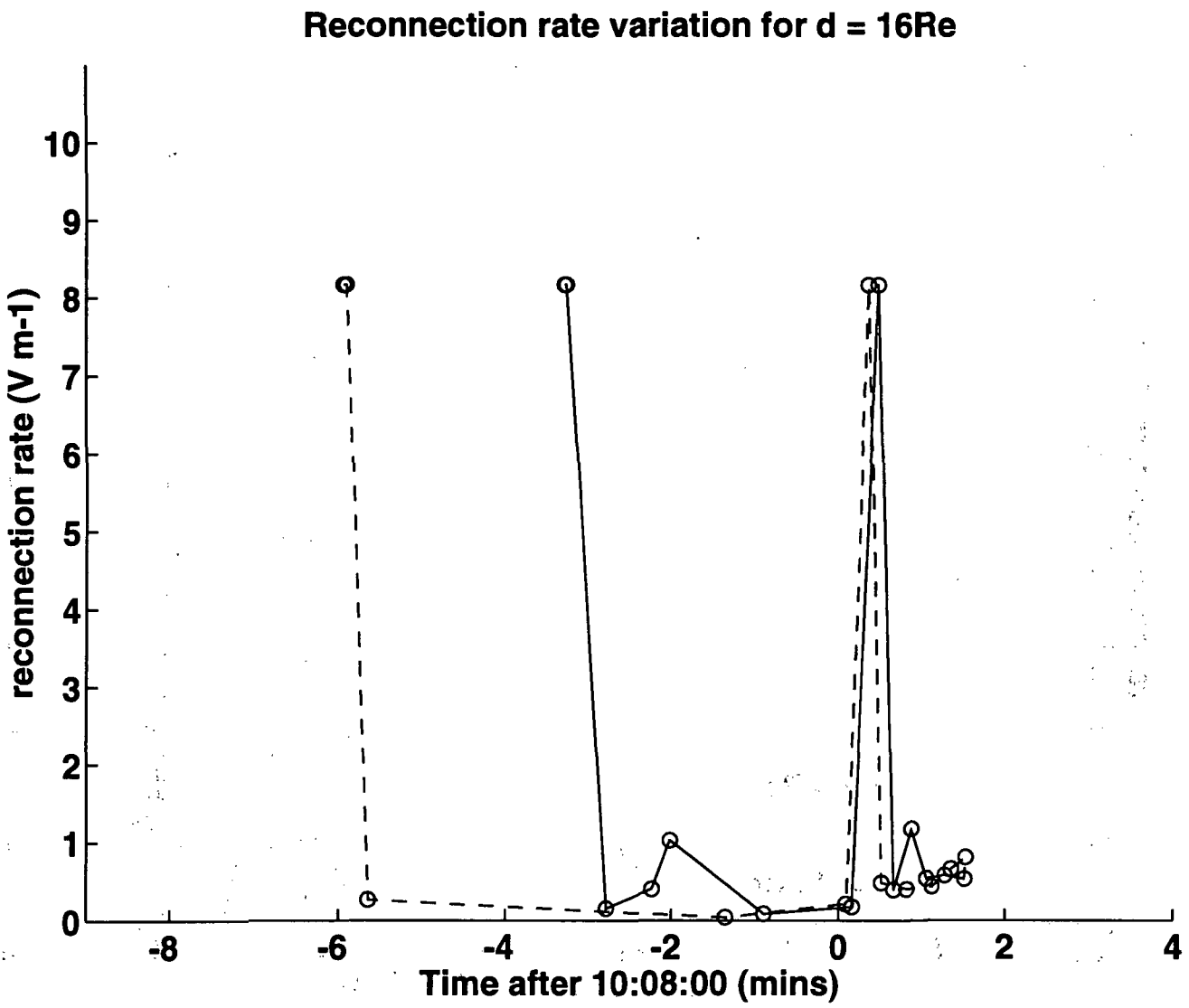
Reconnection rate variation for d = 16Re
reconnection rate (V m-1)
0
1
2
3
4
5
6
7
8
9
10
-8
-6
-4
-2
0
2
4
Time after 10:08:00 (mins)

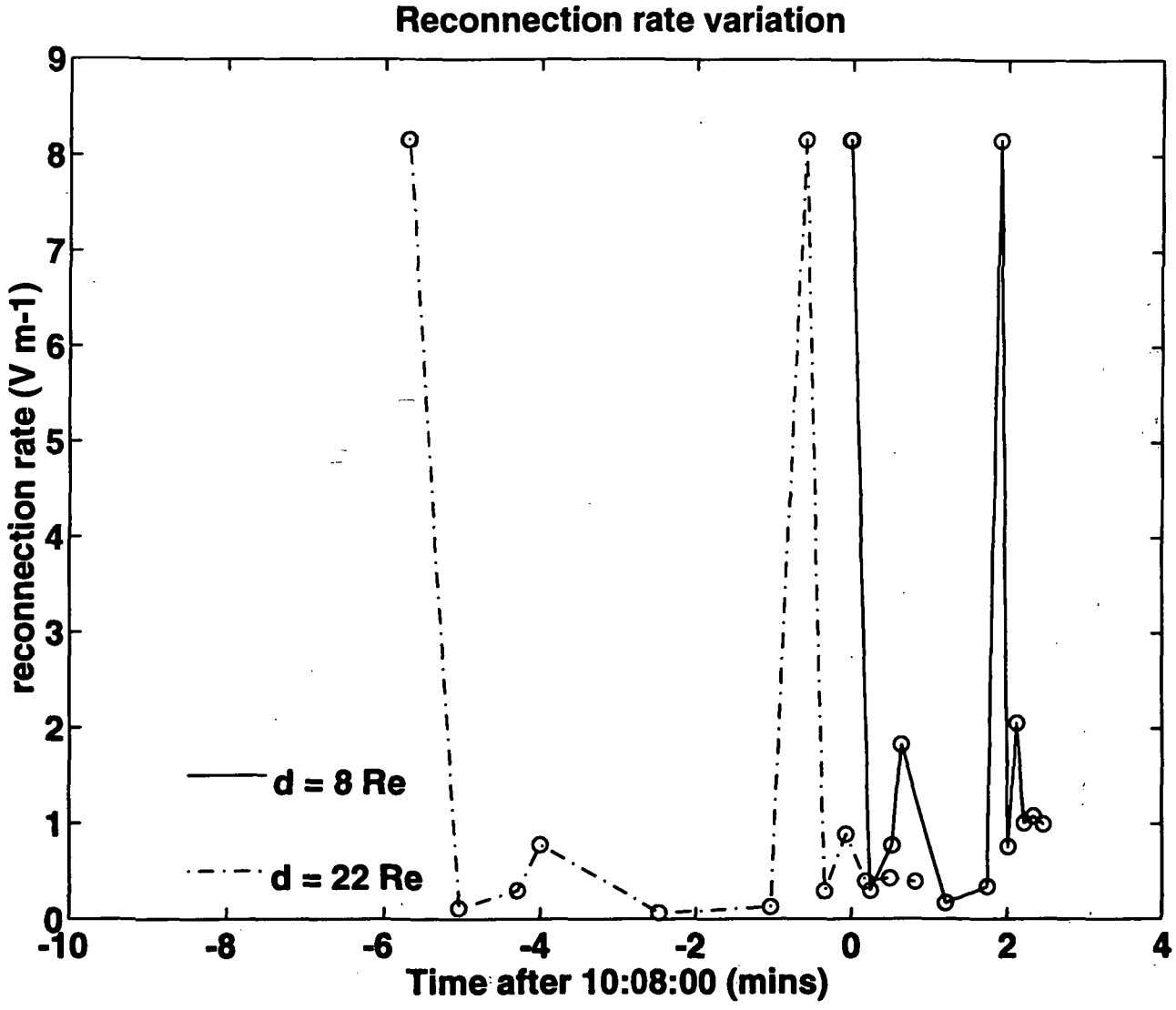
Reconnection rate variation
reconnection rate (V m-1)
Time after 10:08:00 (mins)
d = 8 Re
d = 22 Re
9
8
7
6
5
4
3
2
1
0
-10
-8
-6
-4
-2
0
2
4

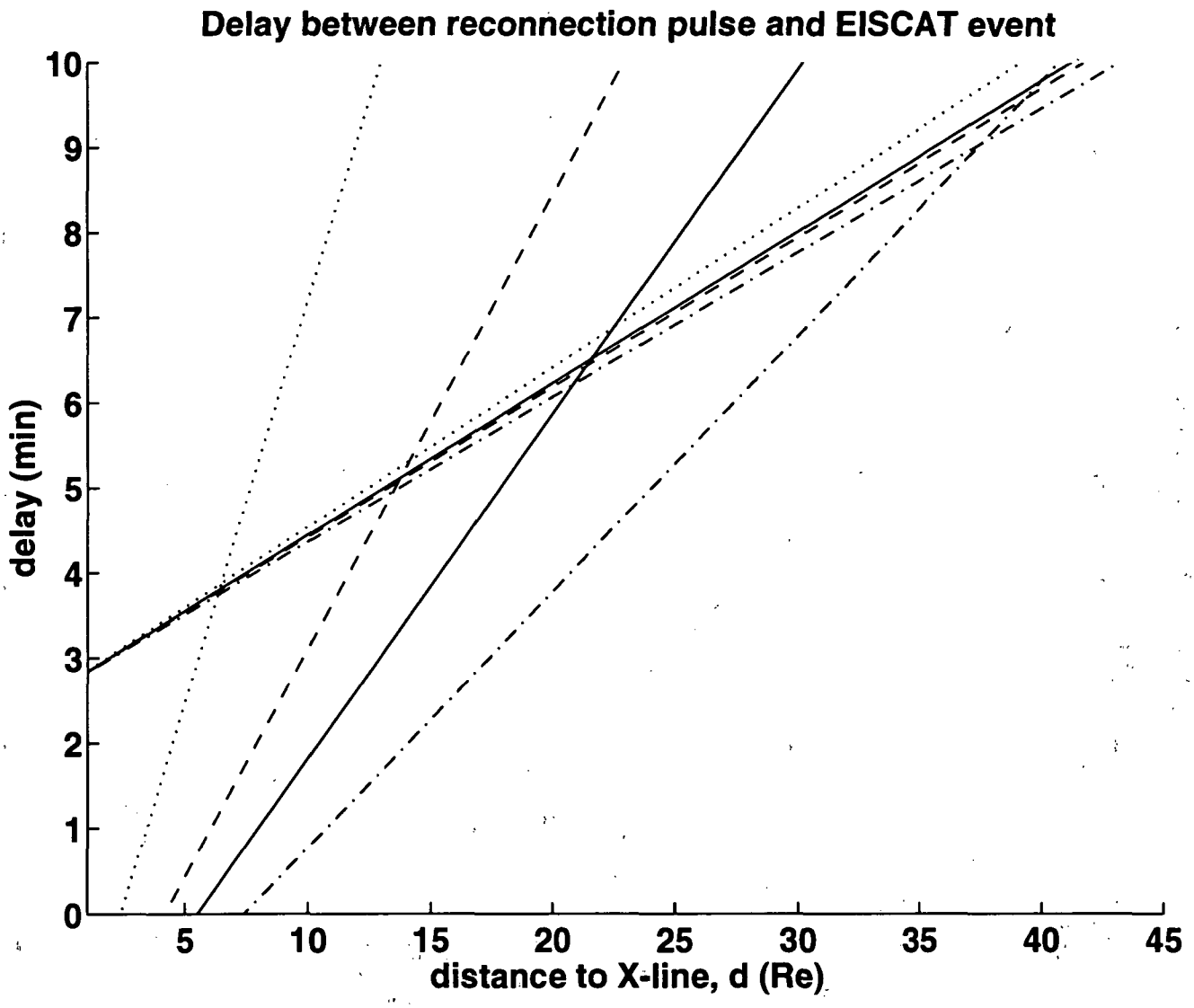
Delay between reconnection pulse and EISCAT event
delay (min)
distance to X-line, d (Re)
0
1
2
3
4
5
6
7
8
9
10
5
10
15
20
25
30
35
40
45

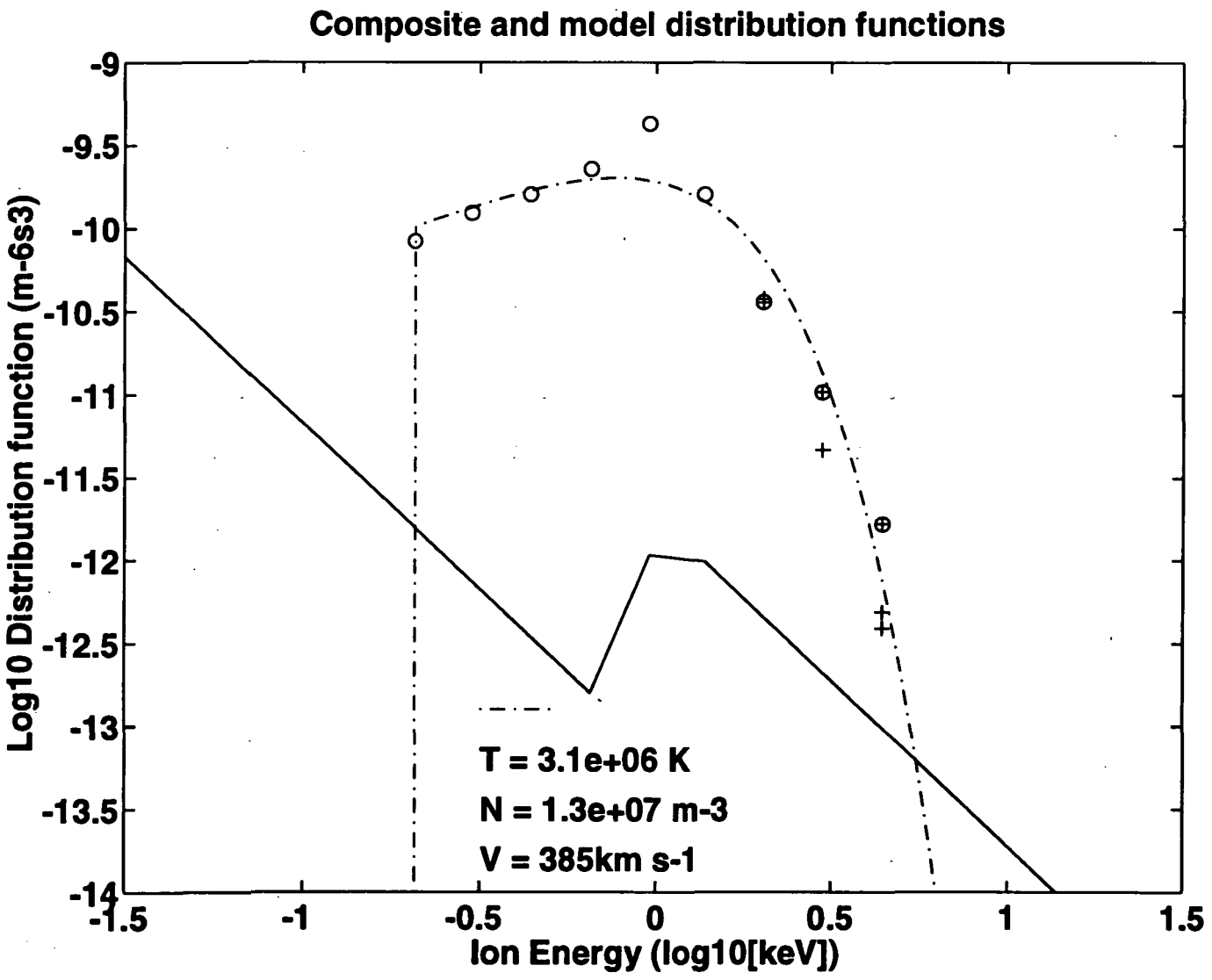
Composite and model distribution functions
Log10 Distribution function (m-6s3)
-9
-9.5
-10
-10.5
-11
-11.5
-12
-12.5
-13
-13.5
-14
-1.5
-1
-0.5
0
0.5
1
1.5
Ion Energy (log10[keV])
T = 3.1e+06 K
N = 1.3e+07 m-3
V = 385km s-1